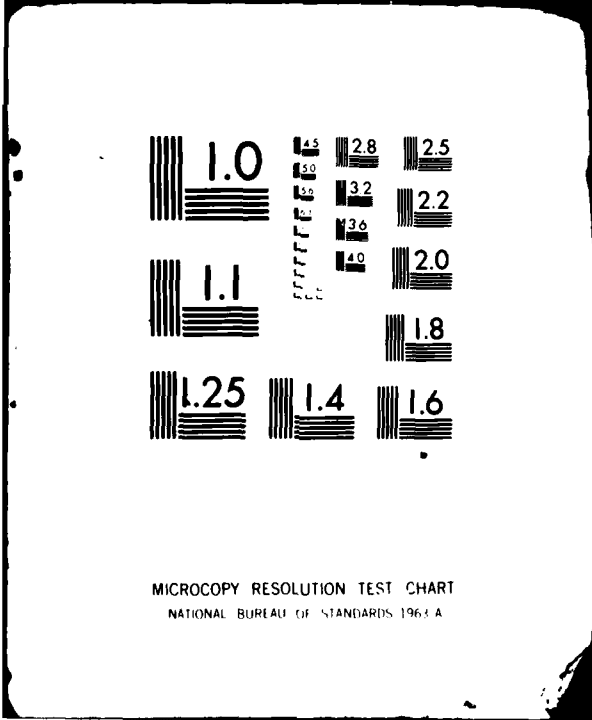


11/41



MICROCOPY RESOLUTION TEST CHART
NATIONAL BUREAU OF STANDARDS 1963-A

ADA111415

Resonance Effects on Shoaling
Surface Gravity Waves

12

FW



DTIC
ELECTE
FEB 26 1982

A

This document has been approved
for public release and sale; its
distribution is unlimited.

Michael Harris Freilich
1982

82 02 26 100

NO COPY

REPORT DOCUMENTATION PAGE		READ INSTRUCTIONS BEFORE COMPLETING FORM
1. REPORT NUMBER	2. GOVT ACCESSION NO. AD-A114 425	3. RECIPIENT'S CATALOG NUMBER
4. TITLE (and Subtitle) RESONANCE EFFECTS ON SHOALING SURFACE GRAVITY WAVES		5. TYPE OF REPORT & PERIOD COVERED PhD Dissertation
		6. PERFORMING ORG. REPORT NUMBER
7. AUTHOR(s) MICHAEL H. FREILICH		8. CONTRACT OR GRANT NUMBER(s) ONR Code 422CS Contract #N00014-75-C-0300
9. PERFORMING ORGANIZATION NAME AND ADDRESS Shore Processes Lab, A-009 Scripps Institution of Oceanography La Jolla, CA 92093		10. PROGRAM ELEMENT, PROJECT, TASK AREA & WORK UNIT NUMBERS
11. CONTROLLING OFFICE NAME AND ADDRESS		12. REPORT DATE 1982
		13. NUMBER OF PAGES 113
14. MONITORING AGENCY NAME & ADDRESS (if different from Controlling Office)		15. SECURITY CLASS. (of this report) Unclassified
		15a. DECLASSIFICATION/DOWNGRADING SCHEDULE
16. DISTRIBUTION STATEMENT (of this Report)		
17. DISTRIBUTION STATEMENT (of the abstract entered in Block 20, if different from Report)		
18. SUPPLEMENTARY NOTES		
19. KEY WORDS (Continue on reverse side if necessary and identify by block number) nonlinear shoaling models, unidirectional surface gravity waves, Boussinesq equations, resonant triad interactions, field experiment, Fourier coefficients dispersion relations, directional spectra, Maximum Likelihood Estimator.		
20. ABSTRACT (Continue on reverse side if necessary and identify by block number) Two nonlinear shoaling models describing the shoaling of unidirectional surface gravity waves are developed. The models, based on variants of the Boussinesq equations for a sloping bottom are cast as a set of coupled evolution equations for the amplitudes and phases of the Fourier modes of the wave field. Resonant and near resonant triad interactions across the entire wind-wave frequency band (0.05-0.25 Hz) provide the mechanism for nonlinear cross spectral energy transfers and phase modifications as the waves propagate (continue over)		

20. (continued)

shoreward through the shoaling region (10 m - 3 m depth). A major field experiment designed to test the operational validity of the models was undertaken in the summer of 1980. Three representative data sets illustrating different initial spectral shape and subsequent evolution are compared in detail to predictions of the shoaling models and linear, finite-depth theory. The nonlinear shoaling models accurately predict Fourier coefficients of the wave field through the shoaling region for all data sets. Differences between the model predictions can be related to differences in the linear dispersion relations of the models. Measurements of directional spectra at two depths are used to partially explain coherence spectra between models and data. The Maximum Likelihood Estimator directional analysis is also used to indicate that seaward-propagating energy in the wind-wave band, although precise limits await design and implementation of a special-purpose, data-adaptive estimator. Finally, some simplifications to the full, nonlinear models are suggested.

UNIVERSITY OF CALIFORNIA

San Diego

Resonance Effects on Shoaling Surface Gravity Waves

A dissertation submitted in partial satisfaction of the
requirements for the degree Doctor of Philosophy
in Oceanography

by

Michael Harris Freilich

Committee in charge:
Professor Robert T. Guza, Chairman
Professor George E. Backus
Professor Russ E. Davis
Professor Myrl C. Hendershott
Professor John W. Miles

1982



Form 50 on file

Dist		
<i>A</i>		

The dissertation of Michael Harris Freilich is approved,
and it is acceptable in quality and form for
publication on microfilm:

George E. Baekus

Bruce E. Part

John W. Miles

Jerry C. Hendrickson

P. T. Snyga

Chairman

University of California, San Diego

1982

To Mom, Dad, Steve, Judy, and Shoshannah

There is always an easy solution to every human problem -
neat, plausible, and wrong.

H. L. Mencken

TABLE OF CONTENTS

	PAGE
LIST OF SYMBOLS	vii
LIST OF FIGURES AND TABLES	x
ACKNOWLEDGEMENTS	xii
VITA and PUBLICATIONS	xiii
FIELDS OF STUDY	xiv
ABSTRACT	xv
I INTRODUCTION	1
II THEORY	7
2.1 The Equations of Motion	8
2.2 A Consistent Shoaling Model	16
2.3 An Alternate Shoaling Model	25
III EXPERIMENT	31
3.1 Site and Instrumentation	31
3.2 Experiment Design and Sensor Placement	35
3.3 Data Acquisition and Reduction	40
3.4 Experiment Overview	43

TABLE OF CONTENTS

	PAGE
IV DATA COMPARISON	45
4.1 Numerical Experiment	47
4.2 The Data	61
4.2.1 5 Sept 80	65
4.2.2 11 Sept 80	76
4.2.3 9 Sept 80	90
V DISCUSSION AND CONCLUSIONS	101
VI REFERENCES	110

LIST OF SYMBOLS

Symbols from the Roman alphabet

a_n	modal amplitude of sea-surface elevation
a_0	typical amplitude (for scaling purposes)
C_g	linear group velocity
C_{pq}	averaged cross spectrum between time series p and q
$D(x_j, t)$	"data" time series from Numerical Example
$\hat{D}(x_j, t)$	"data" Fourier coefficients from Numerical Example
$E(\sigma, \theta)$	frequency-directional spectrum
g	gravity
h	undisturbed water depth
h_0	typical depth (for scaling purposes)
k_n	modal wavenumber
$M_i(x_j, t, T)$	"model" time series from Numerical Example
$\hat{M}_i(x_j, f, T)$	"model" Fourier coefficients from Numerical Example
Q_n	modal amplitude of depth-averaged velocity
$S_i(x_j, t, T)$	"sampled" time series from Numerical Example
$\hat{S}_i(x_j, f, T)$	"sampled" Fourier coefficients from Numerical Example

T_n	nonlinearly-induced modal spatial phase derivative
t	time
x	horizontal (on-offshore) coordinate
z	vertical coordinate

Symbols from the Greek alphabet

α	small expansion parameter (a_0/h_0)
β	small expansion parameter (h_0/λ_0) ²
γ_{pq}	coherence between time series p and q
δ_σ, δ_k	(small) frequency and wavenumber mismatches
ϵ	small expansion parameter
ξ	stretched horizontal coordinate
η	sea-surface elevation
θ_n	total modal phase
θ_{pq}	relative phase between time series p and q
Λ_n	initial modal phase
λ_0	typical wavelength (for scaling purposes)
Ξ	linear differential operator
ζ^\pm	coupling coefficient

ρ	$O(1)$ quantity relating α and β in the shoaling region
σ_n	modal frequency
ϕ	velocity potential
$\overline{\phi}$	depth-averaged velocity potential
ψ_n	modal spatial phase

LIST OF FIGURES AND TABLES

FIGURE		PAGE
1	Definitional sketch of coordinate system	10
2	Plan view of instrument locations	37
3	Averaged power spectra at 6 positions	51
4	"Model" power spectra	54
5	Spectra of coherence	57
6	Spectra of relative phase	59
7	On-offshore bathymetry and sensor locations along the main instrument transect	64
8	Averaged power spectra of SSE measured at 4 on-offshore locations	67
9	Comparison of averaged power spectra	69
10	Comparison of smoothed coherence	72
11	Comparison of relative phase spectra	75
12	Wavenumber vs. frequency for four linear dispersion relations at two depths	78
13	Measured power spectra of SSE for 11 Sept data set	81
14	Comparison of averaged power spectra for 11 Sept data set	83
15	Smoothed coherence spectra for 11 Sept data set	85
16	Spectra of phase between models and data for 11 Sept data set	88
17	Measured power spectra of SSE for 9 Sept data set	92

18	Comparison of averaged power spectra for 9 Sept data set	94
19	Smoothed coherence spectra for 9 Sept data set	97
20	Spectra of phase between models and data for 9 Sept data set	100
21	Frequency-directional spectra in the wind-wave for the 11 Sept data set	104

TABLE		PAGE
I	Positions and approximate uncertainties for sensors in the shoaling waves field experiment	42

ACKNOWLEDGEMENTS

I am deeply indebted to Bob Guza, Bob Lowe, and Steve Pawka. Their advice and insight at all stages of this project greatly enhanced the quality of this work. I am proud and honored to have had the opportunity to work with, and learn from, them. I thank them, and will forever cherish their friendship.

The field experiment would not have been possible were it not for the herculean efforts of Professor D. L. Inman, who has laboriously assembled, at the Shore Processes Lab, the equipment and technical expertise needed to collect detailed and comprehensive data in the nearshore region. The success of the experiment is due to the careful, tireless, and fearless efforts of the students and staff at the Shore Processes Lab. Paul Cunningham, Phil D'Acri, and Dave McLean cheerfully and enthusiastically devoted a seemingly endless summer (March to October) to diving, installing instruments, removing instruments, fixing instruments, stringing cables, etc. Ellick Adler, Bill Boyd, J. C. Boylls, Vanessa Cunningham, Steve Frank, Mike Kirk, Walt Pratt, Martha Shaw, Wayne Spencer, Walt Waldorf, and Joe Wasyl all aided substantially at various stages of the effort. Thank you.

Dr. John Dingler and Professors Ed Thornton and Tony Dalrymple graciously lent me spare pressure sensors.

Shoshannah helped to type the manuscript. Mike Clark drafted some of the figures. To all these and others, my heartfelt thanks.

This research was supported by the Office of Naval Research, Code 422CS (Coastal Sciences), Contract # N00014-75-C-0300. Personal support was provided by a Sea Grant Traineeship, Project # R/CZ-N-4D.

VITA

January 14, 1954 - Born - Philadelphia, Pennsylvania

- 1975 - B.S., Haverford College, Haverford, Pennsylvania
1975 - 1981 Research Assistant, Scripps Institution of Oceanography,
University of California, San Diego

PUBLICATIONS

- Gollub, J.P. and Michael H. Freilich, 1974, Optical heterodyne study of the Taylor instability in a rotating fluid, Phys. Rev. Lett., v 33, p 1465-1468.
- Gollub, J.P. and Michael H. Freilich, 1975, Critical exponents and generalized potential for the Taylor instability, in Fluctuations, Instabilities, and Phase Transitions, T. Riste, ed., p 195-204.
- Gollub, J.P. and Michael H. Freilich, 1976, Optical heterodyne test of perturbation expansions for the Taylor instability, The Physics of Fluids, v 19, p 618-626.
- Flick, R.E., R.L. Lowe, M.H. Freilich, and J.C. Boylls, 1979, Coastal and laboratory wavestaff system, IEEE Oceans, v 79, p 623-625.

FIELDS OF STUDY

Major Field: Oceanography

Studies in Physical Oceanography

Professors R.S. Arthur, C.S. Cox, R.E. Davis, R.T. Guza, M.C. Hendershott, W.H. Munk, and J.L. Reid

Studies in Marine Chemistry

Professor J.M. Gieskes

Studies in Biological Oceanography

Professors J.A. McGowan, R.R. Hessler, M.M. Mullin, and W.A. Newman

Studies in Marine Geology

Professors W.H. Berger and H.W. Menard

Studies in Time Series Analysis

Professor R.A. Haubrich

ABSTRACT OF THE DISSERTATION

Resonance Effects on Shoaling Surface Gravity Waves

by

Michael Harris Freilich

Doctor of Philosophy in Oceanography

University of California, San Diego, 1982

Professor Robert T. Guza, Chairman

Two nonlinear models describing the shoaling of unidirectional surface gravity waves are developed. The models, based on variants of the Boussinesq equations for a sloping bottom (Peregrine (1967)) are cast as a set of coupled evolution equations for the amplitudes and phases of the Fourier modes of the wave field. The models contain no free or empirically determined parameters, and accept arbitrary, broad banded (in frequency) inputs. Resonant and near resonant triad

interactions across the entire wind-wave frequency band (0.05-0.25 Hz) provide the mechanism for nonlinear cross spectral energy transfers and phase modifications as the waves propagate shoreward through the shoaling region (10 m - 3 m depth). A numerical code has been implemented to integrate the coupled evolution equations.

A major field experiment designed to test the operational validity of the models was undertaken in the summer of 1980. Dense instrumentation of the shoaling region provided data on wave parameters over a wide range of conditions. Three representative data sets illustrating different initial spectral shape and subsequent evolution are compared in detail to predictions of the shoaling models and linear, finite-depth theory. The nonlinear shoaling models accurately predict Fourier coefficients of the wave field through the shoaling region for all data sets. Differences between the model predictions can be related to differences in the linear dispersion relations of the models. Slowly varying, linear, finite-depth theory is found to be a poor predictor of Fourier coefficients in regions where significant evolution of the power spectrum of sea-surface elevation was observed, whereas the nonlinear models are good predictors in precisely these regions. However, where such evolution was not observed, linear, finite-depth theory is a superior predictor of both spectral density and phases, thus verifying the validity of the linear, finite-depth dispersion relation in at least some areas of both frequency and physical space in the shoaling region. Nonlinear models such as those derived here are necessary, however, to predict Fourier coefficients over the broad range of wave conditions typically

encountered.

Measurements of directional spectra at two depths are used to partially explain coherence spectra between models and data. The Maximum Likelihood Estimator directional analysis is also used to indicate that seaward-propogating energy in the shoaling region is probably less than 10% of incoming energy in the wind-wave band, although precise limits await design and implementation of a special-purpose, data-adaptive estimator.

Bottom slope is found to influence the nonlinear shoaling transformation only indirectly. Finally, some simplifications to the full, nonlinear models are suggested.

I. INTRODUCTION

As surface gravity waves approach a beach their shapes change dramatically until, in most cases, they break. The aim of the work reported here is to develop and test a model describing the transformations that occur as a spectrum of surface gravity waves propagates shoreward over a mildly sloping bottom. Although wave breaking and subsequent surf-zone fluid motions are both visually spectacular and scientifically important for such processes as sediment transport, the present work will concentrate on the "shoaling region," defined here to be the area between approximately 10m depth and 3m depth, outside and specifically excluding the break zone. On typical Southern California beaches, this shoaling region has a horizontal extent of 300 m to 1000 m. In order to be applicable to field situations, any shoaling model must allow for a complicated wave field characterized by a broad, arbitrarily shaped frequency spectrum. In some areas, due to local beach orientation with respect to the larger scale coastline or offshore topographic features, a realistic shoaling model must also accommodate waves incident at a relatively high angle to the bottom contours at the outer edge of the shoaling region. The models discussed here allow broad frequency spectra but are restricted to waves almost normally incident on a beach with straight, parallel contours. Results from a field experiment at a site satisfying these requirements are used here to test the shoaling models.

Linear theory has often been used as the basis for shoaling wave models. Assuming that the nonlinear terms in the finite-depth,

inviscid, irrotational equations of motion and boundary conditions are small, several authors (Hanson (1926), Friedrichs (1948), Stoker (1957), for a review see Whitham (1979)) have found exact solutions for the case where beach slope h_x is given by $h_x = M\pi/2N$, M and N integers. For the physically interesting case of small bottom slope, approximate (WKB) solutions have been obtained on the assumption of no reflected energy. In these solutions, the wave locally satisfies flat-bottom equations; slow changes in amplitude and phase due to varying depth are obtained by satisfying solubility conditions at the next order in an expansion in bottom slope (Chu and Mei (1970)). The amplitude changes predicted by the WKB solution are of course equal to those obtained by applying conservation of lowest-order energy flux to the lowest order solution (Rayleigh (1911)).

Because of the linear nature of the governing equations, solutions for motions with differing frequencies can be superposed to satisfy any arbitrary conditions at a given on-offshore point. Slowly varying, linear theory is roughly consistent with observations of rms shoaling wave heights (to the 20% level), but some spectral features are apparently due to nonlinear effects (Guza and Thornton (1980)). It seems intuitively clear that the processes immediately preceding wave breaking are essentially nonlinear. As there are well known techniques for incorporating at least weak nonlinearity into a physical problem, attention has naturally turned toward nonlinear aspects of wave shoaling.

Considerable effort has been expended in attempts to use Stokes-type perturbation expansions on the full, finite-depth

equations of motion and boundary conditions for waves over a sloping bottom. (See for instance Skjelbrea and Hendrickson (1960), LeMehaute and Webb (1964), Chu and Mei (1970).) With the exception of Chu and Mei (1970) (who explicitly expand in terms of bottom slope), all dependent variables are expanded in a small parameter (found to be equivalent to the Ursell number $ak/(kh)^3$). Temporally periodic solutions composed of the primary wave and its forced harmonics are found, reducing to the classic Stokes (1847) solution for the case of a flat bottom. The forced harmonics cannot grow to be large (or even comparable) compared with the fundamental. Bottom slope is generally considered to be of a higher order than that to which expansions are carried, and thus WKB energy flux arguments can be applied as in the linear theory. Solutions are steady in the sense that amplitudes of the fundamental and harmonics would not change in the absence of the sloping bottom.

The necessity of the Ursell number remaining small in order to justify the low-order truncation of the series expansion is a particularly stringent restriction for long waves in shallow water characteristic of the shoaling region. The applicability of slowly varying Stokes theory is thus suspect. Fortunately, shallow water approximations to the equations of motion can be derived and have been found to be considerably more tractable. In the limit of very long waves in very shallow water, the classic shallow water equations (Stoker (1957), Whitham (1979)) can be used. Carrier and Greenspan (1958) found an exact solution of these equations for the purely reflective problem of non-breaking waves on a sloping beach. However,

the Carrier and Greenspan solution suffers from restriction to very shallow water in much the same way that the Stokes solutions are essentially restricted to deeper water. Boussinesq (1871) derived a set of evolution equations containing terms accounting for weak dispersion due to finite depth and weak nonlinearity due to finite amplitude. Korteweg and deVries (1895, hereafter K-dV) followed with a single equation describing a similar system supporting unidirectional wave motion only. Both Boussinesq and K-dV obtained exact solutions of their equations describing waves of permanent form in water of constant depth.

Considerable effort in the last two decades has been devoted by others to exploring the limits and applicability of these remarkable systems which not only admit exact, nonlinear, analytic solutions, but also appear to be easily studied in laboratory wave tanks. Starting with Peregrine's (1967) derivation of Boussinesq's equations for mild bottom slope, many authors have conducted extensive experimental and numerical studies of the development and eventual fate of solitary and cnoidal waves over varying bottom topography (see Miles's (1980) review). However, because of the rather restricted initial or boundary conditions required for the exact solutions of Boussinesq- or K-dV-type equations, it is not clear that detailed studies of the behavior of these solutions will lead to a general shoaling model for surface gravity waves.

Wave observations on open and partially sheltered coasts confirm that the frequency and wavenumber spectra of sea-surface elevation and horizontal velocity can vary appreciably on time scales

of days, even when the area of interest is not in an active generation region. Although occasionally incoming wave energy is concentrated in a narrow band of frequencies and directions analogous to the basically monochromatic systems discussed above, most of the time the spectrum is broad or contains multiple peaks (not harmonics). Following the suggestion of Phillips (1960) that energy could be transferred between deep water gravity waves of different frequencies and directions, Hasselmann (1962, 1963, 1966) developed a model for such nonlinear resonant transfers in a general, continuous spectrum of deep water gravity waves. Much additional work followed on this essentially statistical problem (Benney and Saffman (1965), Newell (1968), Willebrand (1975), Longuet-Higgins (1976), Hasselmann and Herterich (1979)). Such work has demonstrated that the quartet resonance mechanism can indeed cause significant changes in the spectrum of the wave field over distances of several hundred kilometers or more. Importantly, although details of the evolution depend on the spectrum, the models themselves do not require a specific initial spectral shape. A major difficulty in the work has been the complication due to the presence of two asymptotic limiting procedures; one due to perturbation expansions in small nonlinearity, and the other due to the passage from discrete to continuous spectra.

Armstrong et. al. (1962) and Bretherton (1964) introduced the idea of "near resonance" in weakly nonlinear systems with discrete spectra. Near resonant systems exhibit behavior similar to resonant systems on moderate scales, but appear more like forced systems on long scales. Mei and Unluata (1972) and Bryant (1973) demonstrated

that Boussinesq-type shallow water equations for waves over a flat bottom support near resonance at second (quadratic) order. Because the near resonance in the equations occurs at lower order than for deep water gravity waves, significant energy transfers and phase modifications can take place in several hundred meters rather than hundreds or thousands of kilometers.

In Chapter II of this work we develop two nonlinear models for the evolution of the wave field in the shoaling region, based on sloping bottom Boussinesq-type equations. The mechanism for the shoaling transformation is seen to be triad near resonance across the entire wind-wave frequency band. The models predict both cross-spectral energy transfers and nonlinear phase changes. Chapter III describes a field experiment in which detailed measurements of wave parameters were collected throughout the shoaling region. Measurements are compared with model predictions for a variety of wave conditions in Chapter IV, and further discussion and conclusions appear in Chapter V.

II. THEORY

In this section we derive equations for the evolution of amplitudes and phases of inviscid, irrotational, wind-waves propagating shoreward over slowly varying, impermeable topography. These rate equations are a consequence of triad near resonance in the governing, shallow water, Boussinesq-type master equations.

To justify the use of shallow water equations, periodic solutions are first found for the special case of linear waves over a flat bottom of arbitrary depth. The dispersion relation obtained indicates that for motions in the wind-wave frequency band defined here as 0.05-0.25 Hz, wavelengths are large compared with the water depth almost everywhere in the shoaling region. This motivates the derivation of a simplified set of nonlinear equations of motion valid only for such long waves. Small amplitude solutions of these equations yield a dispersion relation which is at most only mildly dispersive. We show that such a system supports triad near resonance. Thus amplitudes and phases of lowest order solutions are expected to vary slowly due to nonlinear wave-wave interactions. Two-scale methods are used to solve the nonlinear, long wave equations; at lowest order, the linear, flat-bottom dispersion relation is obtained as well as a relation between sea-surface elevation and velocity potential. Carrying the solution to the next order yields equations for the on-offshore evolution of lowest order amplitudes and phases.

The Equations of Motion

The equations of motion and boundary conditions for the one-dimensional, irrotational motion of an inviscid, incompressible fluid over an impermeable bottom are well known:

$$\begin{aligned}
 \nabla^2 \phi &= 0 & -h(x) \leq z \leq \eta(x,t) & \quad (a) \\
 \phi_z &= -h_x \phi_x & z = -h(x) & \quad (b) \\
 \eta_t + (\eta_x \phi_x) - \phi_z &= 0 & z = \eta(x,t) & \quad (c) \\
 g\eta + \phi_t + \frac{1}{2}(\phi_x^2 + \phi_z^2) &= 0 & z = \eta(x,t) & \quad (d)
 \end{aligned}
 \tag{1}$$

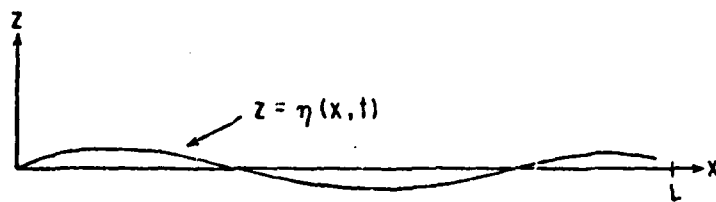
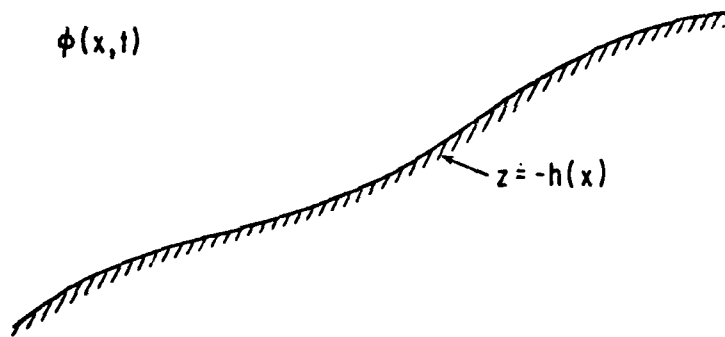
where $\nabla^2 = \frac{\partial^2}{\partial x^2} + \frac{\partial^2}{\partial z^2}$, $-h(x)$ is the bottom, $\eta(x,t)$ is the free surface, and $\phi(x,t)$ is the velocity potential. (See figure (1) for a definitional sketch.) It is possible to nondimensionalize, expand, and scale the system (1) such that the nonlinear terms in the surface boundary conditions (1.c, 1.d) differ from the other terms by the factor $\epsilon = (a_0 \lambda_0^2) / (4\pi^2 h_0^3)$, where a_0 is a typical sea-surface elevation amplitude, λ_0 a horizontal scale of motion, and h_0 a depth. If ϵ and the bottom slope h_x are small, then a solution of the lowest order equations is

$$\begin{aligned}
 \eta &= a \cos(kx - \sigma t) & (a) \\
 \phi &= \frac{ga}{\sigma} \frac{\cosh k(z+h)}{\cosh kh} \sin(kx - \sigma t) & (b) \quad (2) \\
 \sigma^2 &= gk \tanh kh & (c)
 \end{aligned}$$

Evaluation of the dispersion relation (2.c) shows that in 10 m depth (at the outer edge of the experimental shoaling region), even short wind-waves of 4 second period have a wavelength greater than twice the

Figure 1

Definitional sketch and coordinate system

 $\phi(x, t)$ 

water depth. Although the Stokes expansion used to obtain the solutions (2) is correct for deep and moderate depth water (where wavelengths are not much larger than the depth), it is clear that the requirement that the Ursell number ($\sim \epsilon$) remain small will preclude its use in shallow water except for the smallest amplitude wind-waves.

This severe constraint on wave amplitudes can be relaxed if it is assumed a priori that the depth is shallow. The derivations of equations for finite amplitude long waves were originally based on physical arguments (Boussinesq (1871), Korteweg and de Vries (1895)) and later put on firmer formal ground by Friederichs (1948) and Keller (1948). The more formal derivations begin by nondimensionalizing and scaling the horizontal and vertical coordinates in (1) differently. The dependent variables are then expanded in a power series in $(\text{depth}/\text{wavelength})^2$, resulting in two equations corresponding to the boundary conditions (1.c) and (1.d), each with the two small parameters (h_0^2/λ^2) and (a_0/h_0) . Boussinesq's equations are then obtained by retaining terms up to first order in each of these parameters, thus modeling the effects of both weak dispersion and weak nonlinearity. These equations admit exact solutions corresponding to waves of permanent form, the so-called cnoidal and solitary waves. Generalizations of the Boussinesq and K-dV equations to include the effects of sloping bottoms were obtained by Peregrine (1967), Mei and LeMehaute (1966), Ostrovsky and Pelinovsky (1970), Grimshaw (1970), and Johnson (1973). Svendsen and Hansen (1978) discuss the size (in an ordered sense) of bottom slope for which the equations can be expected to remain valid models of the physical system from which they

were derived. Although the solitary and cnoidal wave literature is extensive, to our knowledge no analytic or numerical work has been done pertaining to the transformation, on a sloping bottom, of periodic waveforms of arbitrary spectral shape (within of course, the bounds of long waves). We now give a brief derivation of the sloping bottom Boussinesq equations, following Peregrine (1967) and Grimshaw (1970).

The independent and dependent variables in (1) can be nondimensionalized and scaled by

$$x' = \lambda_0 x; \quad z' = h_0 z; \quad t' = \frac{\lambda_0}{\sqrt{gh_0}} t; \quad h' = h_0 z; \quad \phi' = \frac{g\lambda_0 a_0}{\sqrt{gh_0}} \phi; \quad \eta' = a_0 \eta \quad (3)$$

(where unprimed quantities are nondimensional), resulting in

$$\beta \phi_{xx} + \phi_{zz} = 0 \quad -h \leq z \leq \alpha \eta \quad (a)$$

$$\beta h_x \phi_x + \phi_z = 0 \quad z = -h \quad (b)$$

$$\beta \eta_t + \beta \alpha \eta_x \phi_x - \phi_z = 0 \quad z = \alpha \eta \quad (c) \quad (4)$$

$$\beta \eta + \beta \eta_t + \frac{1}{2} \beta \alpha \phi_x^2 + \frac{1}{2} \alpha \phi_z^2 = 0 \quad z = \alpha \eta \quad (d)$$

$$\alpha = a_0/h_0; \quad \beta = (h_0/\lambda_0)^2 \quad (e)$$

ϕ is then expanded in the form

$$\phi = \phi_0 + \beta \phi_1 + \beta^2 \phi_2 + O(\beta^3) \quad (5)$$

with the forms of ϕ_0 , ϕ_1 , and ϕ_2 obtained by substitution of the expansion for ϕ into (4.a) and (4.b), yielding

$$\phi_0 = \phi_0(x, t) \quad (a)$$

$$\phi_1 = \frac{1}{2} z^2 \phi_{0xx} - z(\phi_{0x} h)_x \quad (b) \quad (6)$$

$$\begin{aligned} \phi_2 = & \frac{1}{24} z^4 \phi_{0xxxx} + \frac{1}{6} z^3 (\phi_{0x} h)_{xxx} + \\ & z \left(\frac{1}{6} h^3 \phi_{0xxx} - \frac{1}{2} h^2 (\phi_{0x} h)_{xx} \right)_x \quad (c) \end{aligned}$$

If the expansion (6) is then substituted into (4.c, 4.d), neglecting terms of $O(\alpha\beta, \alpha^2, \beta^2)$, then the system

$$\eta + \phi_{0t} + \frac{1}{2} \alpha (\phi_{0x})^2 = O(\alpha\beta, \alpha^2, \beta^2) \quad (a)$$

$$\eta_t + (\phi_{0x} h)_x + \alpha (\eta \phi_{0x})_x + \beta \left\{ \left(\frac{1}{3} h^3 \phi_{0xx} \right)_{xx} + \right. \quad (7)$$

$$\left. \frac{1}{2} (h^2 h_{xx} \phi_{0x})_x \right\} = O(\alpha^2, \alpha\beta, \beta^2) \quad (b)$$

is obtained (Grimshaw (1970)). These are the sloping bottom variant of Boussinesq's equations for the surface velocity potential. By repeated use of (5) and (6.a, 6.b), they can be transformed into equations for any desired velocity potential variable. For instance, the average velocity potential is defined by

$$\bar{\phi} \equiv \frac{1}{h + \alpha\eta} \int_{-h}^{\alpha\eta} \phi(x, z, t) dz \quad (a)$$

leading to

(8)

$$\bar{\phi} = \phi_0 - \frac{1}{6} \beta \phi_{0xx} h^2 + \frac{1}{2} \beta h (\phi_{0x} h)_x + O(\beta^2, \alpha\beta) \quad (b)$$

(8.b) can then be inverted and substituted into (7); the resulting

system (after considerable algebra)

$$\eta_x + \bar{\phi}_{xt} - \frac{1}{2} h \beta (\bar{\phi}_{xt} h)_{xx} + \frac{1}{6} h^2 \beta \bar{\phi}_{xxxxt} + \quad (a)$$

$$\frac{1}{2} \alpha (\bar{\phi}_x^2)_x = O(\alpha\beta, \alpha^2, \beta^2) \quad (9)$$

$$\eta_t + (h\bar{\phi}_x)_x + (n\bar{\phi}_x)_x = O(\alpha\beta, \alpha^2, \beta^2) \quad (b)$$

is equivalent to Peregrine's (1967) equations (13, 14). Returning to dimensional coordinates, we obtain as our approximate equations of motion for wind-waves in the shoaling region (dropping primes)

$$g\eta_x + \bar{\phi}_{xt} + \frac{1}{2} (\bar{\phi}_x)^2 = \frac{1}{2} h (\bar{\phi}_{xt} h)_{xx} - \frac{1}{6} h^2 \bar{\phi}_{xxxxt} \quad (a)$$

$$(10)$$

$$\eta_t + (h\bar{\phi}_x)_x + (n\bar{\phi}_x)_x = 0 \quad (b)$$

As there are no explicit restrictions on their applicability, a few comments are warranted. Firstly, equations (10) are good approximations to the full equations (1) only for the case of long waves of moderate nonlinearity

$$O(h_0^2/\lambda_0^2) = O(a_0/h_0) \ll 1$$

In addition, even if these conditions on the parameters of the solution are valid, the equations cannot be considered a valid model for all values of the independent variables; terms of formal order $((h_0/\lambda_0)^4, (a_0/h_0)^2, \dots)$ which were neglected in the equations may have $O(1)$ effects on the solution over nondimensional times and distances $O((h_0/\lambda_0)^{-4}, (a_0/h_0)^{-2})$. This is analogous to the

discrepancies intuitively expected between solutions of inviscid, conservative, equations and the behaviour of "real" (nonconservative), isolated, physical systems. The conservative equations are generally derived by an ordering process (explicit or implicit) equivalent to that shown above, with the viscous terms deemed to be of higher order. Solutions of the conservative system will be apparently valid for all values of the independent variables. In fact, we expect that the real effect of the neglected viscosity will be to cause the isolated system to lose energy to its surroundings, and thus eventually to "run down." The details of the energy loss processes and their effects on the system can never be inferred from solutions of the conservative equations.

Additionally, one can view the neglected terms as adding errors of their order into any local solution. On ordering grounds, even exact solutions of the approximate equations cannot be expected to be exact solutions of the full equations of motion obeyed by a real system. It is thus wholly consistent with the derivation of approximate equations to pursue approximate solutions (which have a more obviously limited validity) in an attempt to model specific phenomena. This is true even when, as in the present case, exact solutions of the approximate equations can be obtained for a limited class of initial or boundary conditions.

A Consistent Shoaling Model

The equations (10) can be recast as a set of approximate equations describing the spatial evolution of the Fourier modes of the wave field. The resulting equations are valid for a wave field that is everywhere periodic in time in a region of length L (large compared with a wavelength, but not larger than the a priori limits on the validity of (10) discussed above). In the following, the implicit assumption $\alpha = \beta$ used in the derivations of (9) and (10) is made explicit upon renormalizing by the substitution $\beta = \rho\alpha$ ($\rho = O(1)$ is the inverse of the Ursell number, $\rho = h_0^3 k_0^2 / a_0$). Mild and slowly varying bottom slope is made explicit by the assumption $h = h(\alpha x)$; then $\frac{\partial^n h}{\partial x^n} = O(\alpha^n)$. The equations in nondimensional form then become

$$\eta_x + \bar{\phi}_{xt} - \frac{1}{3} \rho \alpha h^2 \bar{\phi}_{xxxxt} + \frac{1}{2} \alpha (\bar{\phi}_x^2)_x = 0 \quad (a)$$

$$\eta_t + (\bar{\phi}_x h)_x + \alpha (\eta \bar{\phi}_x)_x = 0 \quad (b) \quad (11)$$

$$\text{on } 0 \leq x \leq L, \quad L \leq O(\alpha^{-2}), \quad \alpha \ll 1 \quad (c)$$

Before embarking on the protracted algebra required for a perturbation-type solution of (11), it is instructive to investigate the linearized form of (11) obtained by allowing $\alpha = 0$:

$$\bar{\phi}_t + \eta = 0 \quad (a)$$

$$\eta_t + h \bar{\phi}_{xx} = 0 \quad (b) \quad (12)$$

This set is just the linear shallow water equations for a flat bottom

(Stoker (1957)). Periodic solutions of (12) of the form

$$\eta = a \cos(kx - \sigma t + \Lambda) \quad (a) \quad (13)$$

$$\bar{\phi} = Q \sin(kx - \sigma t + \Lambda) \quad (b)$$

yield the relations

$$Q = a/\sigma \quad (a) \quad (14)$$

$$k = \sigma/h \quad (b)$$

The linear dependence of k on σ in the dispersion relation (14.b) indicates the well known fact that linear, shallow water waves are nondispersive, with all frequencies propagating at a uniform phase speed that depends only on the (nondimensional) depth. This has important consequences on higher order (in α) solutions of (11). At next order, the nonlinear terms in (11) appear, and there arises the possibility of either nonlinearly generated forced waves or resonant triads. Which manifestation of the nonlinearity actually occurs depends on the form of the lowest order dispersion relation.

Second order, forced waves are due to nonlinear interactions among lowest order, free waves, resulting in time and space periodicities that are incommensurate with the lowest order dispersion relation. Forced wave amplitudes are constrained to be always small, of $O(\alpha)$.

If, however, nonlinear interactions between lowest order free modes result in motions that satisfy the dispersion relations, nonlinear resonance occurs. The requirement that nonlinear

interactions between lowest order modes result in resonant forcing is expressed by the "resonance conditions"

$$\begin{aligned} \pm \sigma_1 \pm \sigma_2 - \sigma_3 &= 0 & (a) \\ \pm \vec{k}_1 \pm \vec{k}_2 - \vec{k}_3 &= 0 & (b) \end{aligned} \tag{15}$$

where each (σ_n, k_n) satisfies the lowest order dispersion relation. Clearly, if motion is unidirectional and the dispersion relation relating $|k|$ and σ is linear, (15.a) and (15.b) are not independent constraints. Under these conditions, if one of (15.a) or (15.b) is satisfied, then the other must be satisfied as well. Thus triad interactions governed by equations (11) must be resonant. The literature on resonances in general is extensive (for a review of physically interesting triad resonances, see Kaup et. al, (1979 a,b); Hasselmann (1966) enumerates geophysical resonances; while Phillips (1974) reviews resonances in waves in fluids.) The salient features of the interactions are:

- 1) $O(1)$ energy can be slowly (on length scales large compared with wavelengths) transferred between interacting modes;
- 2) Similarly and simultaneously, slow phase shifts (equivalent to small changes in the phase speeds) can occur among the interacting modes.

The scales on which significant nonlinear energy or phase changes can occur is approximately (α^{-1}) , where α is the (small) measure of the size of the nonlinear terms (Bretherton (1964), Phillips (1977)).

Bretherton (1964) and Armstrong et. al. (1962) used methods similar to the two-scale technique of Krylov and Bogoliubov (see Minorsky (1974) or Cole (1968)) to obtain asymptotic solutions describing resonant interactions. In the following, similar techniques will be employed to derive approximate solutions of (11).

We expand the dependent variables $\bar{\phi}, \eta$ in a power series in α :

$$\bar{\phi} = \bar{\phi}_1 + \alpha \bar{\phi}_2 + \dots \quad (a)$$

$$\eta = \eta_1 + \alpha \eta_2 + \dots \quad (b)$$

(16)

The solution will be carried only as far as the first term in each expansion. Anticipating resonant interactions, we will allow parameters of the solutions $\bar{\phi}_1, \eta_1$, to vary slowly with x . Specifically, assume solutions of the form

$$\bar{\phi}_1 = \sum_n Q_n(x) \sin(\psi_n(x) - \sigma_n t) \quad (a)$$

$$\eta_1 = \sum_n a_n(x) \cos(\psi_n(x) - \sigma_n t) \quad (b)$$

(17)

where $\sigma_n = n\Delta\sigma$ and Q_n, a_n are functions of the slow space variable $\xi = \alpha x$ (similar to $h = h(\alpha x)$) such that

$$\frac{d^n}{dx^n} \begin{pmatrix} a_n \\ Q_n \end{pmatrix} = \alpha^n \frac{d^n}{d\xi^n} \begin{pmatrix} a_n \\ Q_n \end{pmatrix} + O(\alpha^{n+1}) \quad (18)$$

The spatial phase function $\psi_n(x)$ has both $O(1)$ derivatives (corresponding to the basic wave motion itself) and higher order derivatives (slow phase changes due both to the sloping bottom and to

the anticipated effect of resonant interactions):

$$\frac{d}{dx} \psi_n(x) = k_n(\xi) + \alpha T_n(\xi) + O(\alpha^2) \quad (a)$$

$$\frac{d^2}{dx^2} \psi_n(x) = \alpha \frac{d}{d\xi} k_n(\xi) + O(\alpha^2) \quad (b)$$

When (17)-(19) are substituted into (11), the lowest order relations (14) are obtained. Higher order solutions are more compactly pursued if (11.a, 11.b) are cross-differentiated and subtracted to eliminate linear terms containing n :

$$\begin{aligned} \bar{\phi}_{1xtt} - h\bar{\phi}_{1xx} - \frac{1}{3} \rho a h^2 \bar{\phi}_{1xxx} + \frac{1}{2} \alpha (\bar{\phi}_{1x}^2)_{xt} - \\ 2 \alpha h \xi \bar{\phi}_{1xx} - \alpha (n \bar{\phi}_{1x})_{xx} = 0 \end{aligned} \quad (20)$$

Substitution of (17)-(19) into (20) yields at $O(\alpha)$

$$\begin{aligned} \sum_n \{ Q_{n\xi} (3hk_n^2 - \sigma_n^2) + Q_n k_n (3hk_{n\xi} + 2h_\xi k_n) \} \sin \theta_n + \\ \sum_n \{ Q_n T_n (3hk_n^2 - \sigma_n^2) - \frac{1}{3} \rho h^2 Q_n k_n^3 \sigma_n^2 \} \cos \theta_n + \\ \frac{1}{2} \sum_{j,m} Q_j Q_m k_m (k_j + k_m) \{ \frac{1}{2} k_j (\sigma_j + \sigma_m) + \sigma_j (k_j + k_m) \} \cos(\theta_j + \theta_m) + \\ \frac{1}{2} \sum_{j,m} Q_j Q_m k_m (k_j - k_m) \{ \frac{1}{2} k_j (\sigma_j - \sigma_m) + \sigma_j (k_j - k_m) \} \cos(\theta_j - \theta_m) \\ = \Xi(\phi_2) \end{aligned} \quad (21)$$

where $\theta_q = (\psi_q - \sigma_q t)$ and Ξ is the linear operator

$$\Xi \equiv \left(\frac{\partial^3}{\partial x \partial t^2} - h \frac{\partial^3}{\partial x^3} \right).$$

If all waves are unidirectional, then (14.b) can be used to eliminate

k. The technique of Krylov and Bogoliubov, essentially a solubility constraint, requires that ϕ_2 not contain time periodicities common to ϕ_1 . Since the sums in (21) are taken over all (positive) frequencies, ϕ_2 can thus be set identically equal to zero. Then, applying the resonance condition (15.a) and making use of the fact that all frequencies are harmonics of a small frequency $\Delta\sigma$,

$$\begin{aligned} \sum_n \{2Q_n \xi \sigma_n^2 + Q_n (\frac{1}{2} \sigma_n^2 \frac{h\xi}{h})\} \sin \theta_n + \sum_n Q_n \sigma_n^2 \{2T_n - \frac{1}{3} \rho \sqrt{h} \sigma_n^3\} \cos \theta_n = \\ - \frac{3}{4}(h)^{-\frac{3}{2}} \sum_{jn} \{Q_j Q_{(n-j)} \sigma_j \sigma_{(n-j)} \sigma_n^2 \sin(\theta_j + \theta_{(n-j)})\} \quad (22) \\ - \frac{3}{4}(h)^{-\frac{3}{2}} \sum_{jn} \{Q_j Q_{(j-n)} \sigma_j \sigma_{(j-n)} \sigma_n^2 \sin(\theta_j - \theta_{(j-n)})\} \end{aligned}$$

Expanding the arguments $\theta_j \pm \theta_{\pm(n-j)}$, adding and subtracting ψ_n , and equating like frequencies, two evolution equations for each mode are obtained:

$$Q_{n\xi} = -\frac{1}{2} Q_n \frac{h\xi}{h} + \sum_j Q_j Q_{(n-j)} \left\{ \frac{3}{8}(h)^{-\frac{3}{2}} \sigma_j \sigma_{(n-j)} \right\} \sin(\psi_j + \psi_{(n-j)} - \psi_n) + \quad (a)$$

$$\sum_j Q_j Q_{(j-n)} \left\{ \frac{3}{8}(h)^{-\frac{3}{2}} \sigma_j \sigma_{(j-n)} \right\} \sin(\psi_j - \psi_{(j-n)} - \psi_n) \quad (23)$$

$$T_n = \frac{1}{6} \rho \sqrt{h} \sigma_n^3 - \sum_j \frac{Q_j Q_{(n-j)}}{Q_n} \left\{ \frac{3}{8}(h)^{-\frac{3}{2}} \sigma_j \sigma_{(n-j)} \right\} \cos(\psi_j + \psi_{(n-j)} - \psi_n) -$$

$$\sum_j \frac{Q_j Q_{(j-n)}}{Q_n} \left\{ \frac{3}{8}(h)^{-\frac{3}{2}} \sigma_j \sigma_{(j-n)} \right\} \cos(\psi_j - \psi_{(j-n)} - \psi_n) \quad (b)$$

The problem is thus reduced to solving the system (23) of coupled, first order, ordinary differential equations for modal amplitudes and phases.

If it is assumed that all energy in the shoaling region is propagating shoreward (thus specifically neglecting reflection in the shoaling region), knowledge of the Fourier coefficients of sea-surface elevation and velocity potential at a single on-offshore location provides a sufficient boundary condition for solution of the evolution equations. Boundary conditions of the form

$$\bar{\phi}_1(0,t) = \sum_n Q_n^- \cos(\Lambda_n + \sigma_n t) \quad (a)$$

$$\eta_1(0,t) = \sum_n a_n^- \cos(\Lambda_n + \sigma_n t) \quad (b) \quad (24)$$

$$\sigma_n = n\Delta\sigma$$

are used to set the integration constants $Q_n(0)$, $\psi_n(0)$. The solution $\bar{\phi} = \bar{\phi}_1 + O(\alpha^2)$ is a first order solution uniformly valid over the horizontal extent $0 \leq x \leq L$, $L < O(\alpha^{-2})$. For larger values of x , the cumulative effects of the neglected derivative terms $\frac{d^n}{dx^n} \begin{pmatrix} Q_j \\ \tau_j \end{pmatrix}$, $n \geq 2$, are expected to invalidate the solution. Furthermore, terms of this formal order have been omitted from the basic equations (9, 10) so that higher order solutions are pointless unless higher order versions of (9, 10) are properly derived.

Some physical meaning can be given each of the terms on the RHS of (23.a,b). The first term of (23.a) has the form of "linear shoaling," that is, the result due to a WKB solution of the linear equations (12) on a mildly sloping bottom. It is present due to the

assumption that bottom slope is $O(\alpha)$. If bottom slope was deemed of higher order, the term would not appear in these equations, but it would appear in exactly the same form in a higher order solution.

The first term of (23.b) models the effect of $O(\alpha)$ dispersion. The term represents an increase in phase speed that is dependent weakly on depth and strongly on frequency, and is precisely the first correction to an expansion of the linear, finite-depth dispersion relation (2.c) for small kh .

The remaining terms in (23.a, b) are due to nonlinear, resonant triad interactions. Since they are a sum over all possible interactions in which a given mode can participate, they represent the net rate of change of modal amplitude and phase. Viewed heuristically, a mode can be simultaneously participating in one triad in which it is gaining energy and in another in which it is losing energy. The ordering criterion of slow modal amplitude and phase changes must be satisfied for both the net changes and each individual triad interaction. Each of the interaction terms is composed of a quadratic product of amplitudes, a coupling coefficient, and a trigonometric term whose argument is a function of spatial phases only. In the case of phases (23.b), the terms are further divided by the amplitude of the mode of interest. Phases thus have "amplitude inertia" in that small amplitude modes will tend to experience larger phase shifts due to nonlinear interactions than will larger amplitude modes (all else remaining equal). Note that if the dimensionless amplitude of any mode starts and remains small ($O(\alpha)$) for many interaction lengths, the formal ordering scheme is technically

violated. Such a situation occurs for initial conditions described by narrow-banded power spectra. In such cases, models similar to (23) predict only small, nonlinearly-induced changes in the amplitudes and phases of modes whose frequencies are not near harmonics of the spectral peak. Although inclusion of such modes in $O(\alpha)$ rate equations such as (23) is not justified, comparisons between measured data and the formally inconsistent predictions of (23) are seen to be remarkably good (cf. section 5.2.2).

The coupling coefficients do not depend on either the amplitudes or phases of the interacting waves, but are functions (in general) of their frequencies, wave numbers, and the local depth. For a given resonant triad, the value of the coupling coefficient increases with decreasing depth.

The trigonometric term modulates the amplitude and phase changes according to the relative spatial phases of the three waves in a given triad. At a position $x=D'$, the relative phase can be written

$$\psi_j \pm \psi_{\pm(n-j)} - \psi_n = \int_0^{D'} \frac{d}{dx} (\psi_j \pm \psi_{\pm(n-j)} - \psi_n) dx +$$

$$\psi_j(0) \pm \psi_{\pm(n-j)}(0) - \psi_n(0)$$

Using the definition (19.a) and the dispersion relation,

$$\psi_j \pm \psi_{\pm(n-j)} - \psi_n = \int_0^{D'} \alpha (T_j \pm T_{\pm(n-j)} - T_n) dx +$$

$$(\psi_j(0) \pm \psi_{\pm(n-j)}(0) - \psi_n(0))$$
(25)

The importance of nonlinear phase changes over large distances is manifest in the integral on the RHS of (25). Although the integrand is formally $O(\alpha)$, if D' is $O(\alpha^{-1})$, the integral contributes an $O(1)$

amount to the relative phase. This affects both the magnitude and sign of the amplitude and phase changes undergone by the interacting waves. Effects of the linear dispersion term in (23.b) are also expressed through the trigonometric modulation terms. Dispersion causes the phases of higher frequency modes to change more quickly in x than those of low frequency modes (independent of nonlinear interactions). The relative phase of a triad containing high frequency modes will thus oscillate more rapidly than one containing only low frequency modes. Consequently, the value and sign of the trigonometric term will change more quickly, and net (over a distance $D' < L$) energy transfers and phase modulations will be smaller.

An Alternate Shoaling Model

The dimensional equations (10) can also be nondimensionalized and scaled by:

$$x' = h_0 x; \quad t' = \sqrt{\frac{h_0}{g}} t; \quad \eta' = a_0 \eta; \quad \phi' = a_0 \sqrt{gh_0} \phi; \quad h' = h_0 h \quad (26)$$

yielding:

$$\bar{\phi}_{xt} + \frac{1}{2} \epsilon (\bar{\phi}_x^2)_x + \eta_x - \epsilon h h_\xi \bar{\phi}_{xxt} - \frac{1}{3} h^2 \bar{\phi}_{xxx} = 0 \quad (a)$$

$$\eta_t + \epsilon h_\xi \bar{\phi}_x + h \bar{\phi}_{xx} + \epsilon (\eta \bar{\phi}_x)_x = 0 \quad (b)$$

where $\epsilon = a_0/h_0 \ll 1$ and bottom slope is $O(\epsilon)$. This set of equations, used by Mei and Unluata (1972) (the nondimensionalization and scaling was apparently used implicitly by Peregrine (1972) in deriving his

"linearized Boussinesq equations") has only the nonlinear terms explicitly small; the dispersive term $\frac{1}{3} h^2 \bar{\phi}_{xxxxt}$ is formally $O(1)$. The equations for $\epsilon = 0$ yield the counterpart of (14),

$$Q = \frac{a\sigma}{hk^2} \quad (a)$$

(28)

$$k = \frac{\sigma}{\sqrt{h}} \left(1 - \frac{1}{3} h\sigma^2\right)^{-\frac{1}{2}} \quad (b)$$

The wave number k is no longer a linear function of σ . However, if $\frac{1}{3} h \sigma^2 \ll 1$, (28.b) can be expanded and truncated to

$$k = \frac{\sigma}{\sqrt{h}} \left(1 + \frac{1}{6} h\sigma^2 + O(h^2\sigma^4)\right)$$

and the leading term is just shallow water dispersion. In terms of dimensional coordinates, the restriction of

$$\frac{1}{3} h\sigma^2 \ll 1$$

is not very severe for the physical shoaling problem. $\frac{1}{3} h\sigma^2 = 0.3$ corresponds to wave period about 6 seconds in 10 m depth, 4 seconds in 5 m depth, and a value of $(\text{depth/wavelength})^2$ (β of the previous discussions) of about 0.04. Thus although the system (27) formally has lowest order dispersion, for the wavelengths and frequencies encountered in the physical shoaling problem, the dispersion is mild. In the following, we will ignore the formal ordering problems associated with the fact that, with the present scaling, realistic values of σ and k will be small and will use the full dispersion relation (28.b). Similar selective failure to neglect formally high order terms is not uncommon in the literature (eg. Grimshaw (1970) and Bryant (1973)), and occasionally has led to erroneous conclusions (cf.

Johnson's (1973) comments regarding Grimshaw (1970)). In Chapters IV and V we will present experimental evidence that suggests that the major differences between a shoaling model (30) (derived from equations (27)), and the model (23) (derived from (9)), are attributable to differences in linear dispersion relations. WKB, finite-depth, linear theory will be seen to yield the best predictions of power spectra and average phase in the "linear" regions of physical and frequency space where differences between the two nonlinear models are most apparent. As the linear dispersion relation (28.b) is a better model of the finite-depth relation (2.c) than is (14.b), equations (27) will in fact be seen to provide a slightly better model for predictions of power spectra of sea-surface elevation than the more consistent equations (9).

Bretherton (1964) showed that a system such as (27), with only mild dispersion, can be treated analytically by the methods described earlier for exactly resonant systems. Monotonic dispersion prohibits (in general) any triad from satisfying both resonance conditions (15) exactly. However, if the dispersion is mild, (15) can be satisfied with only small error by some triads. The conditions for this "near resonance" are:

$$\pm \sigma_1 \pm \sigma_2 = \sigma_3 + \delta_\sigma \quad (a)$$

$$\pm \vec{k}_1 \pm \vec{k}_2 = \vec{k}_3 + \vec{\delta}_k \quad (b) \quad (29)$$

$$|\delta_\sigma|, |\vec{\delta}_k| = O(\epsilon) \quad (c)$$

The formalism of (16)-(23) can be easily carried through (in the present case, $\delta_\sigma = 0$); the resulting evolution equations are:

$$Q_{n\xi} = - \frac{Q_n k_n^2 h_\xi (3\sigma_n^2 - 1)}{2 \sigma_n^2} + \sum_j \frac{1}{2} Q_j Q_{(n-j)} \zeta^+(j,n) \sin(\psi_j + \psi_{(n-j)} - \psi_n) +$$

$$\sum_j \frac{1}{2} Q_j Q_{(j-n)} \zeta^-(j,n) \sin(\psi_j - \psi_{(j-n)} - \psi_n) \quad (a)$$

$$(30)$$

$$T_n = - \sum_j \frac{Q_j Q_{(n-j)}}{4Q_n} \zeta^+(j,n) \cos(\psi_j + \psi_{(n-j)} - \psi_n) -$$

$$\sum_j \frac{Q_j Q_{(j-n)}}{4Q_n} \zeta^-(j,n) \cos(\psi_j - \psi_{(j-n)} - \psi_n) \quad (b)$$

where $\zeta^\pm(j,n) \equiv k_j k_{\pm(n-j)} (k_j \pm k_{\pm(n-j)}) \{ h \frac{k_j}{\sigma_j} (k_j \pm k_{\pm(n-j)}) + \frac{1}{2} \sigma_n \}$.

(Equation (30) can be simplified and the coupling coefficients made symmetric by omitting terms of $O(\delta_k = \epsilon)$.) The physical explanation of most terms is the same as for equations (23). However, (30.b) lacks a linear phase shift. The effect is modeled, in this case, by the $O(1)$ dispersion through the dispersion relation relating k to σ . The relative phase terms now have argument

$$\psi_j \pm \psi_{\pm(n-j)} - \psi_n = \int_0^{D'} (k_j \pm k_{\pm(n-j)} - k_n) dx +$$

$$\int_0^{D'} \epsilon (\tau_j \pm \tau_{\pm(n-j)} - \tau_n) dx + (\psi_j(0) \pm \psi_{\pm(n-j)}(0) - \psi_n(0))$$

By (29.b) above, $(k_j \pm k_{\pm(n-j)} - k_n) = O(\epsilon)$; on a flat or mildly sloping bottom where the wave numbers are only slowly varying functions of x ,

the effect of the mismatch in the resonance condition is to introduce slow changes in the relative phase of the triad similar to the linear phase shift term in (23.b). The larger the mismatch, the more rapid the phase oscillations. Since the deviation from linearity of the dispersion relation (and hence the mismatch) is more pronounced at high frequency, the net energy transfers and phase changes are small for triads containing high frequency waves. It is thus reasonable to suppose that a high frequency cutoff in the sums (17) is possible; as long as it is sufficiently high, the exact cutoff frequency is not critical (Bretherton (1964)). Of course, as depth decreases, the waves become more nondispersive in character. In the limit of extremely small depth, all high frequency modes have vanishing mismatch, and the cutoff frequency must be extremely high (c.f. Nayfeh (1981)). In this case, however, both the governing equations (10) and the perturbation-solution techniques are inappropriate and should be replaced by the nonlinear shallow water equations (Stoker (1957)) and one of the many techniques for obtaining approximate solutions of hyperbolic equations (Whitham (1974), Nayfeh (1981)).

Neither system (23) nor (30) have known analytic solutions. If the depth is constant and only a single resonant triad is considered, Armstrong et. al. (1962) and Bretherton (1964) show that a solution exists in which modal amplitude and phase variations are described by Jacobi elliptic functions. These solutions are applicable to a broad spectrum of modes only in the case where ϵ becomes so small that any given mode participates in at most a single (near) resonant triad (Bretherton (1964)). This is clearly not the

case for shoaling surface gravity waves. The evolution equations must thus be integrated numerically.

In the present study we have implemented a numerical integration scheme known as "repeated extrapolation to the limit" due to Gragg (1963) and Bulirsch and Stoer (1966) (see Stoer (1972) for a review of extrapolation methods and improvements on the algorithm published in Bulirsch and Stoer (1966)). The algorithm is both efficient and highly accurate and is easily modified to accommodate large numbers of coupled equations. We have performed considerable testing to verify the accuracy of the numerical scheme. Four coupled equations (corresponding to the amplitudes and phases of a fundamental and its second harmonic) were integrated over a flat bottom for more than a kilometer (in dimensional coordinates) for both equations (30) and (23). The results were compared with the analytic solution expressed in terms of Jacobi elliptic functions (Armstrong et. al. (1962)). Modal amplitudes differed from the exact solution by less than 0.5% everywhere, and phases by less than 0.1 radian, over a variety of initial amplitudes and phases. In addition, internal consistency checks were carried out for integrations of up to 30 modes. The automatic step size feature of the algorithm was disabled, and integrations were performed with a range of basic step sizes. All results compared well (less than 1% maximum difference) for step sizes over a range of a factor of 5.

III. EXPERIMENT

A field experiment to measure the wave parameters of sea-surface elevation, pressure, and horizontal velocity was undertaken at Torrey Pines Beach, Ca., during the summer and fall of 1980. The primary goal of the field work was to determine the operational validity of the one-dimensional shoaling models developed in the previous section. However, the dearth of existing quantitative wave measurements in the shoaling region motivated an extension of purpose. A secondary goal was to provide a comprehensive, quantitative description of wave-induced fluid motions throughout the shoaling region, with the hope that the data would be useful for validating future theories. To this end, the on-offshore measurements were extended beyond the defined shoaling region (10 m depth to 3 m depth), and two longshore arrays of instruments at different depths were established to allow measurement of wave frequency-directional spectra.

This chapter describes the experimental site and types of instruments used, experiment design and sensor placement, data acquisition and reduction, and concludes with a brief overview of the data set as a whole.

Site and Instrumentation

Torrey Pines Beach, Ca. has been the site of numerous nearshore field experiments (Pawka et. al. (1976), Aubrey (1978), Gable (1979), Inman et.al. (1980)). Located approximately 3 km north

of Scripps Pier, it is readily accessible both by small boat and four-wheel-drive vehicle. The bathymetry is relatively homogeneous in the longshore direction, with contours running approximately 6.5° west of true north-south. The beach is composed of fine, quartz sand (mean diameter 0.17 mm) and has a fairly constant slope of about 2% through the instrumented region. An extensive study of the wave climate at the site was reported by Pawka et. al. (1976).

In all, 28 channels of wave data were obtained from three types of instruments: 10 pressure sensors, 5 dual-axis, electromagnetic, current meters, and 8 surface-piercing wavestaffs. The pressure sensors used were of the strain gauge type, predominantly Statham model PA 506-33 (a limited number of Transducer Inc. #5AP-69F-50 were also used). The pressure sensors are extremely durable and easy to install and maintain when mounted in the standard configuration, approximately 25 cm above the bottom. Previous experience has shown them to be highly linear and drift free over long periods of time and varying ocean conditions. All instruments were pre- and post-calibrated with agreement to better than 3%. Raw pressure signals were amplified prior to being digitized, resulting in least count error of 0.003 m.

The linearized form of Bernoulli's equation can be used to relate pressure signals directly to sea-surface elevation or horizontal speed when finite amplitude effects are locally small. Pawka (1976) and Guza and Thornton (1980) present comparisons between estimations of wave parameters derived from co-located pressure sensors, wavestaffs, and current meters throughout the shoaling region

and surf zone. In most cases reported, agreement between pressure-derived estimates of sea-surface elevation and direct measurements was well within 10% in amplitude across the entire wind-wave frequency band. The agreement is virtually independent of spectral shape, total energy, and on-offshore position, with the exception of the region near the break zone. In place of the linear, finite-depth transformations, the relations obtained from the linear Boussinesq equations can also be used with comparable results everywhere except at high frequencies (> 0.17 Hz) in deep water (> 9 m). The discrepancy is due to breakdown of the long wave assumption inherent in the derivation of the Boussinesq equations. The linear, finite-depth theory was therefore used to transform between bottom pressure and sea-surface elevation.

The current meters were Marsh-McBirney #512 dual-axis, electromagnetic, current meters. The instruments measure two orthogonal components of velocity. In this experiment, the sensing elements were placed approximately one meter above the bottom, and horizontal velocity (longshore, on-offshore) was measured. Although rugged and durable, there is considerable uncertainty about the dynamic response of the instruments to a broad-banded wave field (Lavelle (1978), Cunningham et. al. (1979)). Additional uncertainty in orientation (about 5° in all directions) further degrades the current meter data. The performance of the E-M current meters was a disappointment throughout the course of the experiment. Apparent gain reductions of up to 30% were observed to occur over immersion periods of about a month. The changes became apparent only when new, dry,

meters were substituted for ones that had been underwater for some time. Because of the questionable gain, it was initially decided to ignore all current meter data for comparison with the shoaling models presented here. Since various types of instruments were intermingled on the on-offshore line, the loss of all current meter data was not catastrophic. It did, however, seriously affect the high-frequency aliasing characteristics of the directional arrays, as the current meters were the basis for the shortest on-offshore lag in each array.

The wavestaffs used were similar to those described in Flick et. al. (1979), consisting of twin resistance wires supported vertically by a 5 m long fiberglass pole. They are useful for direct measurements of sea-surface elevation in depths shallower than about 6 m. As with pressure sensors, considerable field testing has shown these instruments to be linear and stable, with excellent frequency response up to 10 Hz. Although post-calibrations were not possible due to breakage of the sensing wires in the storm of 1-2 October, each instrument had been calibrated periodically for more than a month prior to being installed, with differences at the 1% level for gain and offset. In addition, wavestaffs and pressure sensors were "in situ" calibrated by comparing predicted and observed tides and intercomparing mean depths between sensors over time. Least count error for the wavestaffs was less than 0.002 m. The largest source of error in the measurements was due to the staff being mounted at an angle to true vertical. Visual and photographic observations showed that the staffs were well within 20° of vertical, resulting in elevation errors less than 6%.

Experiment design and sensor placement

Quantitative comparison of the one-dimensional shoaling models' predictions with data required instrumentation of an on-offshore transect through the shoaling region, approximately 300 m in horizontal extent. Based on the results of Guza and Thornton (1980), spatial coverage was maximized by placing only a single instrument at each on-offshore location; the linear, finite-depth relations were used to locally transform from the measured variable to the wave variable of interest on a frequency band-by-band basis.

Previous data obtained on the same beach in November, 1978, as well as casual observation, indicated that the evolution of the frequency spectrum became more pronounced in shallow water than in the deeper regions of the shoaling region. This is entirely consistent with the form of the evolution equations (23) and (30), in which wave amplitudes, coupling coefficients, and closeness to resonance, all increase with decreasing depth. Trial comparisons of spectral evolution between numerical integrations of the evolution equations and November, 1978 field data indicated qualitative agreement. Additional model testing with idealized, synthetic, input conditions confirmed the trend toward increased spectral shape evolution with decreasing depth. Thus, rather than sampling evenly along the on-offshore transect, the density of instruments was greater in shallow water, primarily at the expense of mid-depth (8-6 m) regions. As seen in the plan view figure (2), a mix of 4 pressure sensors, 5 current meters, and 3 wavestaffs constituted the main on-offshore instrumentation. Wavestaffs were used in shallow water in place of

Figure 2

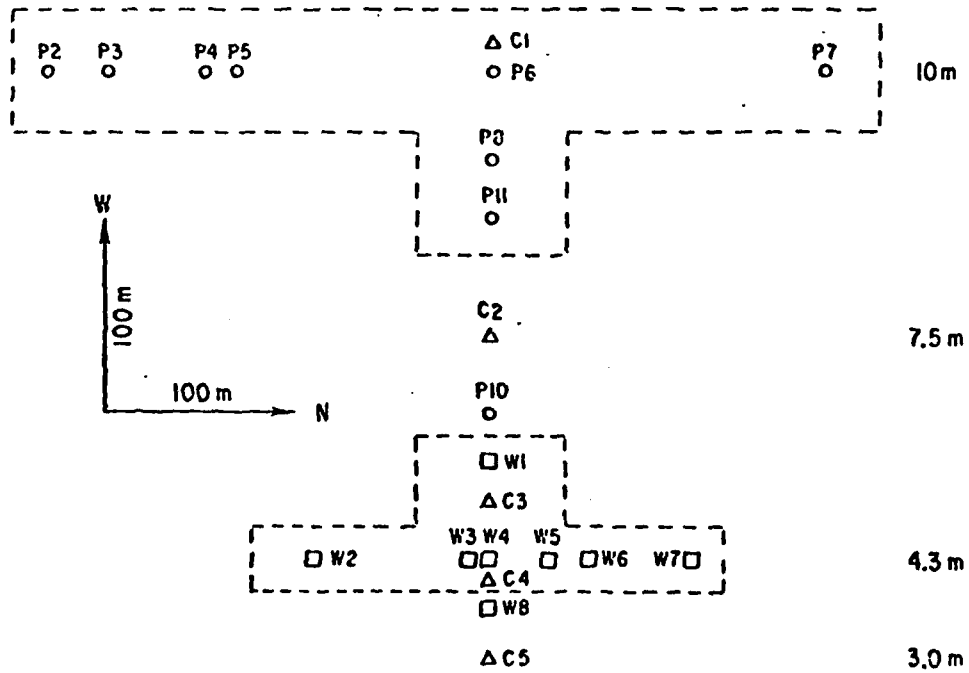
Plan view of the instrument locations in the 1980 shoaling waves field experiment. Approximate depths are given near the right side of the figure.

SHOALING WAVES EXPERIMENT

○ P1

14 m

- = PRESSURE SENSOR
- △ = CURRENT METER
- = WAVESTAFF



pressure sensors, in part to avoid complications arising from previously observed discrepancies near the break zone between direct measurements of sea-surface elevation and estimates inferred from pressure data; however, under most wave conditions the instrumentation did not extend to the break zone.

An additional pressure sensor (P1) was placed approximately 240 m seaward of P6 in a depth of 14.5 m. P1 was placed 4.3 m above the bottom, considerably higher in the water column than other sensors, in order to maximize the frequency range of acceptable signal to noise. If evolution of the wave field was truly dominated by near resonant triad interactions as hypothesized, such interactions were expected to be very weak over large portions of the wind-wave frequency band in water deeper than 10 m. At these relatively large depths, quantitative predictions of the Boussinesq models were expected to diverge from actual data, in consequence of the breakdown of the long wave assumptions crucial to the derivation of the models. Qualitatively, however, the increased inability of the wave field to satisfy the triad resonance conditions was expected to hinder net nonlinear transfers via the triad mechanism. As discussed in Chapter I, nonlinear energy exchanges should then occur on the much larger length scales appropriate to the quartet mechanism of Phillips (1960) and Hasselmann (1962). The primary function of the deep sensor P1 was to verify this qualitative reasoning.

The field experiment was designed to measure wave directional spectra quantitatively at two depths in the shoaling region. A well-surveyed, 5 sensor linear array of pressure sensors comprising

instruments P2, P3, P5, P6, and P7 (see figure (2)) had been established at the Torrey Pines site in March, 1977. Design criteria and analysis techniques for this array are discussed in detail by Pawka (1981). The array had a total longshore extent of 400 m. The original five sensor array had minimum lag spacing of 33 m, corresponding to an aliasing frequency of 0.16 Hz in 10 m depth (Pawka, 1981). Addition of another sensor (P4) for the present experiment reduced the minimum lag to 17.8 m and the aliasing frequency to 0.20 Hz. This is approximately the high frequency limit imposed by depth extinction of the pressure signal itself. Addition of P4 also allowed use of the four sensor subarray P2-P3-P4-P5, with optimal spacing 1-3-2 (Barber (1961)), in the event that sensor locations P6 and P7 could not be supported; however, the anticipated problems did not materialize, and use of the shortened array was not necessary.

All linear wave-gauge arrays suffer from 180° directional ambiguity with respect to the line connecting the sensors. The historical justification for the use of linear longshore arrays in coastal regions has been the assumption, which was avoided here, of no seaward-propagating energy in the wind-wave frequency band. In the plan view figure (2), all sensors enclosed within a set of dashed lines were designed to be analyzed as a single, two-dimensional, directional array. Such an array theoretically allows unambiguous resolution between seaward- and shoreward-propagating energy in a given frequency band. Some results of directional analysis will be discussed in Chapter V; model testing using realistic, synthetic,

directional spectra and the Maximum Likelihood Estimator was used to aid in array design.

A second directional array was designed to operate in a mean depth of approximately 4 m. The heart of this instrument group was a 1-3-2 longshore array of wavestaffs, with basic lag of 10 m. The array thus had aliasing characteristics similar to those of the deep array. Provision was made for two additional sensors in the longshore, and model testing with realistic spectra led to the final longshore array design 8-1-3-2-5, with total length 190 m. Three additional on-offshore sensors (W1, C3, C4) could be included in the analysis to provide full, two-dimensional estimates of the directional spectrum, as with the deep array.

With the exception of a few previously established sensor sites, all sensor locations were initially established using a mini-ranger radar locating system operated from a small boat. Positions were later verified by numerous mini-ranger surveys and direct measurements between instruments. In addition, all wavestaff locations were further refined by shooting redundant sets of angles between the staffs and known benchmarks on the beach. The position and approximate uncertainty for each sensor is given in table (I).

Data Acquisition and Reduction

For data acquisition purposes, the sensors were divided into two groups, based on their on-offshore positions. All sensors seaward of P11 inclusive (see figure (2)) received their power from, and returned signals to, a tethered spar as described by Lowe et. al.

Table I

Positions and approximate uncertainties for sensors in the shoaling waves field experiment. Positions are given in meters relative to a left-handed coordinate system centered on an arbitrary benchmark on the beach, with the positive Y axis aligned with true North (thus approximately longshore). Uncertainties are given in meters, and apply to both X and Y coordinates.

TABLE I

NAME	X	Y	UNCERT
P1	794.6	475.6	4.0
P2	527.5	270.0	0.5
P3	531.6	300.9	0.5
P4	536.4	351.5	0.5
P5	538.1	369.2	0.5
P6	553.4	501.5	0.5
P7	573.4	665.2	0.5
P8	507.0	506.2	1.5
P10	389.0	518.3	2.0
P11	478.9	509.0	1.5
C1	567.4	500.1	1.0
C2	425.0	514.1	2.0
C3	337.6	523.9	1.0
C4	301.8	529.8	0.5
C5	227.7	516.0	2.0
W1	359.9	520.9	0.3
W2	296.9	439.0	0.3
W3	307.7	516.5	0.3
W4	308.5	527.7	0.3
W5	310.3	557.3	0.3
W6	313.8	575.3	0.3
W7	320.8	629.2	0.3
W8	287.3	528.2	0.3

(1972) and Gable (1980). An electronics package inside the spar scanned each data channel at 64 Hz. On each scan, all analog data was digitized, encoded using pulse code modulation, multiplexed, and transmitted over a VHF radio link to the Shore Processes Lab, where the telemetered data stream was recorded on magnetic tape.

A similar scheme was used for data from all sensors shoreward of P11. An underwater electronics package located near location W4 distributed power and performed signal conditioning. Digitized, encoded, multiplexed data was returned to a beach installation via a single cable. The data stream was then transmitted over a separate VHF telemetry link to SPL, where it was recorded on magnetic tape simultaneously with the deep station's data. In a separate, non-real-time operation, data from the raw telemetry tape was decoded, demultiplexed, block averaged to a sampling rate of 2 Hz, and placed onto computer compatible magnetic tape. Further preliminary processing removed "glitches" (caused, for example, by temporary telemetry signal losses) and applied a low-pass, digital filter, with cutoff frequency 0.9 Hz.

Experiment Overview

Useful data was collected sporadically from 14 June 1980 to 1 October 1980. All pressure sensors and wavestaff W1 were operational throughout this period. At most times after 20 June, wavestaff W4 functioned, and W8 (either as a wavestaff or a co-located pressure sensor) came on line after 14 July. Due to difficulties involving wavestaff maintenance and sand accretion, the longshore array of

wavestaffs did not return data reliably until 3 September. However, from this time until 1 October, all pressure sensors and wavestaffs (with the exception of P10 on 4 September) returned high quality data.

The data presented and analyzed in the following chapters was taken over a two week period in early September, 1980. During this time, all pressure sensors and wavestaffs were operational. Continuous data was obtained for between 10,000 seconds and 26,000 seconds on 11 occasions. Tidal variations during data runs ranged between 20 cm and 100 cm (runs were taken across all stages of the tide cycle). Average variance of sea-surface elevation in the wind-wave frequency band (as measured in 10 m depth) was approximately 90 cm^2 in early September, grew to 510 cm^2 on 11 September as wave energy from a storm in the southern hemisphere arrived, and then gradually decreased to 175 cm^2 by 16 September. Spectral shape varied considerably over the two weeks of interest. An intensive bathymetric survey was conducted on 9 September, and measurements of instrument heights off the bottom indicated that the bathymetry of the shoaling region remained relatively constant throughout the two weeks of interest.

IV. DATA COMPARISON

In this chapter we present comparisons between data obtained in the field experiment, predictions of the nonlinear shoaling models (30) and (23), and predictions of linear, finite-depth theory (LFDT). Before presenting the comparisons, however, the relationship between deterministic models and (possibly) stochastic data is explored briefly. By examining some numerical examples, it is found that time series analysis techniques applicable to stochastic processes yield accurate results when applied to deterministic time series composed of many discrete modes. We further demonstrate that nonlinear model predictions of Fourier coefficients (or time series) are relatively insensitive to the number of modes used to describe the wave field.

Finally, by treating the outputs of deterministic models as realizations of a stochastic process, comparisons are made between theories and data for power spectra of sea-surface elevation through the shoaling region. Correlations between model predictions and data are analyzed in the frequency domain by considering coherence and phase spectra of sea-surface elevation. Both of the nonlinear models (30) and (23) accurately predict significant, observed, nonlinear evolution of the power spectrum of sea-surface elevation, while LFDT obviously does not. Coherences and phases between all three models and data are favorable in those regions of frequency space containing large amounts of energy. However, coherences and phases between LFDT and data indicate poor correlation in those regions (both in frequency and on-offshore position) where nonlinear spectral evolution is observed to take place, in contrast with the models (30) and (23),

which continue to have moderately high coherence and near-zero phase difference.

A fundamental problem, both conceptual and operational, involves defining the basic deterministic or stochastic nature of the wave field itself. The models (30) and (23) described in Chapter II are deterministic - they assume that the wave field is composed of a finite number of discrete modes, each having a definite amplitude and phase. On the other hand, the ocean wave field has in recent years been considered a stochastic process. Such processes cannot be characterized by fixed frequencies with definite amplitudes and phases, but must instead be described in a statistical sense. Rather than attempting to give exact values for physically measurable quantities, a statistical description appropriate to a stochastic process attempts to define the probability that the measurable quantities will fall within some range of values. If a deterministic model is perfect (it exactly predicts all physically measurable quantities), it can also be used to answer any statistical questions to any desired precision. Since stochastic models only describe the statistics of quantities, they cannot yield information on the actual values of the quantities themselves. It thus seems desirable to model physical processes deterministically rather than stochastically whenever possible.

It is impossible, given finite data, to determine beyond doubt that a given process is either deterministic or stochastic. As a well known example (see, for instance, Feigenbaum (1980)), a random number generator on a digital computer is clearly a deterministic process

whose outputs can be predicted exactly if the algorithm and seed are known. Yet, if such information is absent or imprecisely known, a finite-length output series (shorter than the repeating block) can pass all tests for "stochasticity"; the output series can, with high probability, be considered a realization of a truly random process with certain statistical properties only. Similar behavior has been found for the outputs of deterministic models of physical systems (Lorenz (1963), Ford (1975), Feigenbaum (1980)). Such models have the property that although they possess very few degrees of freedom, their outputs can at times pass tests for stochasticity if the inputs and model equations are not known precisely.

Numerical Experiment

The numerical examples described in this section are intended to illustrate two points. Firstly, we show, using a time series typical of those measured in the field, that spectral analysis techniques (strictly valid only when applied to realizations of stochastic processes) give quantitatively accurate results when applied to deterministic time series which are underresolved. Thus, given short sections of a deterministic time series, fast Fourier transform techniques, followed by frequency and ensemble averaging of power estimates, can be used to accurately predict the average power in a given frequency band.

Secondly, we demonstrate that deterministic models such as (23) yield similarly accurate predictions of averaged power in a spectral band, as well as having high coherence and near-zero phase

with "data" time series and Fourier coefficients, almost independent of the number of modes used to represent the wave field.

A model data set was constructed with a fixed, large (960), number of modes evenly spaced in the frequency band 0.0002-0.2344 Hz. Initial modal amplitudes and phases were determined by Fourier transforming a 4096 second data record collected at location P6 on 9 September 1980 (see below for an in-depth discussion of this data set). The model "shoaling region" for the numerical experiment was considered to be of constant, 5 m depth, and 283 m in horizontal extent. The 960 modes were taken to represent the initial wave field exactly, and the waves themselves were assumed to obey equations (23) identically. The "data set" consisted of Fourier coefficients of sea-surface elevation $\hat{D}(x_j, f)$ at each of 7 locations x_j , obtained by numerically integrating equations (23) subject to the initial conditions described above. The constant-depth system has significant computational advantages over the more realistic sloping-bottom system. The qualitative nature of the solutions of the flat-bottom system was not expected to be different from solutions over a mildly sloping bottom, as in practice, bottom slope terms were numerically small compared to nonlinear terms under conditions similar to this data set. The 5 m depth was chosen arbitrarily as being representative of the physical shoaling region. The 7 on-offshore positions x_j were chosen to correspond approximately to the positions of sensors in the field experiment.

In the following discussion, each of the time series $D(x_j, t)$ (obtained by inverse transforming the set $\hat{D}(x_j, f)$) will be considered

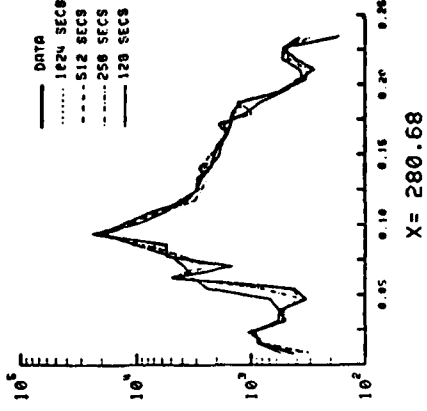
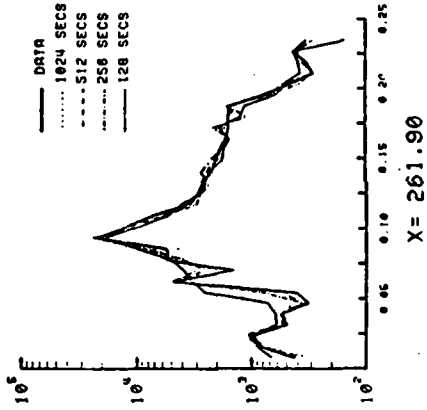
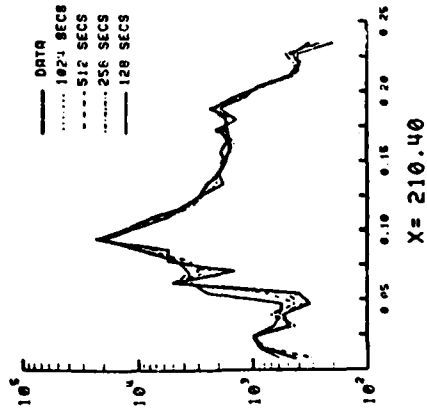
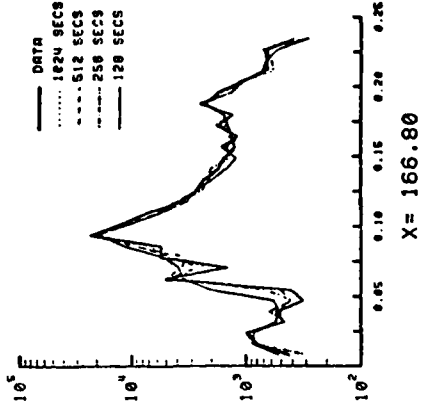
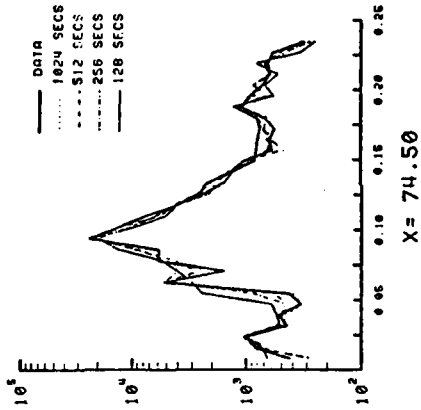
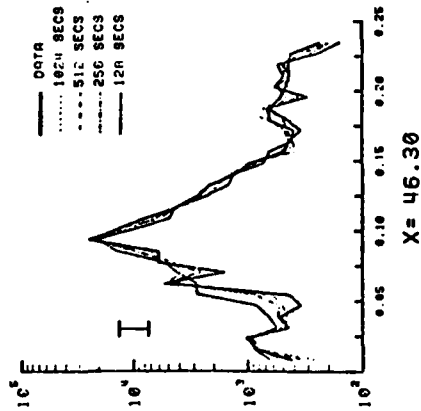
a realization of an ergodic process. Each of the series $D(x_j, t)$ can be broken into shorter records, each of length T , represented by $S_i(x_j, t, T)$. Here the subscript i denotes the "record number" of S , the i th record containing data from times $(i-1)T \leq t < (i)T$. Each of the records $S_i(x_j, t, T)$ can be FFT'd to yield Fourier coefficients at the harmonic frequencies n/T , $n=1, 2, \dots$. If this is done for the records $S_i(x_j, t, T)$, the coefficients $\hat{S}_i(x_j, f, T)$ can serve as initial conditions for an integration of equations (23), thus generating model coefficients $\hat{M}_i(x_j, f, T)$ and time series $M_i(x_j, t, T)$.

If the spectrum of an ergodic process is sufficiently smooth over a chosen bandwidth $1/T$, and low frequency energy is sufficiently small, then equivalent, smoothed, spectral estimates for bandwidth $1/\tau$ can be constructed by ensemble-averaging estimates from records of length at least τ , frequency averaging, or a combination of both. Figure (3) demonstrates that spectral estimates obtained in these ways are indeed equivalent for the time series $D(x_j, t)$ and $S_i(x_j, t, T)$ for $T=128, 256, 512, \text{ and } 1024$ seconds. Presented are smoothed spectra of sea-surface elevation (bandwidth=.00781 Hz, 64 dof) at 6 locations x_j , $j=2, 7$. The data spectrum at each location corresponds to spectra obtained from $\hat{D}(x_j, f)$, frequency-averaged by 32 bands. The other spectra are derived from $\hat{S}_i(x_j, f, T)$ with various values of T , by ensemble- and frequency-averaging. With the exception of the shortest record length $T=128$ seconds, all spectra are quantitatively similar (for reference, the 90% confidence limits on spectral estimates, assuming the process $D(x_j, t)$ is Gaussian, are also plotted). Although frequency-merging of power spectral estimates is pointless for known

Figure 3

Averaged power spectra at 6 positions. "DATA" is from $D(x_j, f)$, frequency-averaged by 32 bands. Other spectra are the result of combinations of frequency- and ensemble-merging of power estimates from Fourier coefficients $S_i(x_j, f, T)$, $T=1024, 512, 256, \text{ and } 128$ seconds. The ordinate of all plots is dimensional frequency (Hz), and the abscissa is spectral density (cm^2/Hz). All spectra have 64 dof, and the 90% confidence limits (identical for all plots) are shown for $x = 46.3 \text{ m}$.

DATA SPECTRA (NUMERICAL EXPERIMENT)



deterministic time series, figure (3) demonstrates that for typical, underresolved data, reasonable estimates of average power in a frequency band can be obtained by treating the data as a realization of a stochastic process without being able, in fact, to prove that the data is random rather than deterministic.

Figure (4) presents a similar comparison between spectra obtained from the model integrations $\hat{M}_i(x_j, f, T)$ and the data $\hat{D}(x_j, f)$. Once again, all spectra are quantitatively similar. In fact, smoothed spectra obtained from $\hat{S}_i(x_j, f, T)$ and $\hat{M}_i(x_j, f, T)$ are virtually identical over all bands at all locations, even though significant spectral evolution with x is observed. It thus seems plausible that for smoothed spectral predictions, the model (23) (and, presumably, similar models such as (30)) are stable with respect to the number of modes used to represent the wave field, if initial modal amplitudes and phases are obtained by Fourier transforming sampled time series such as $S_i(x_j, t, T)$.

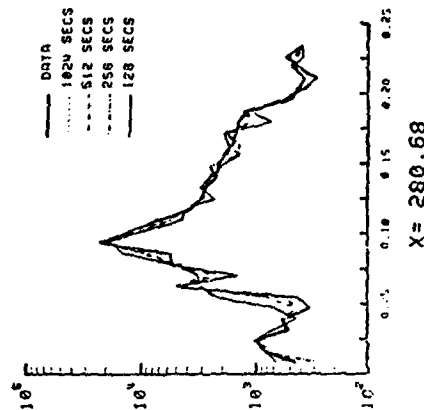
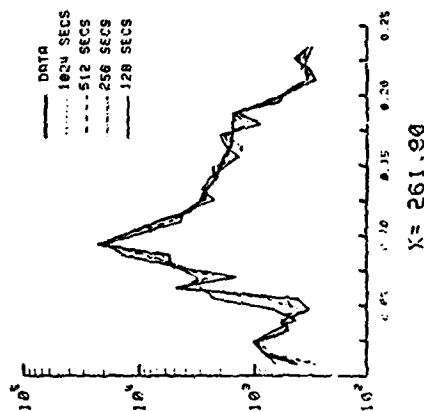
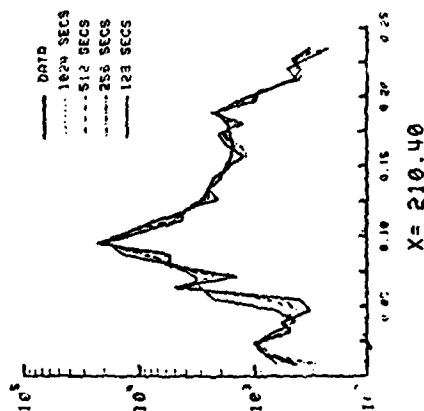
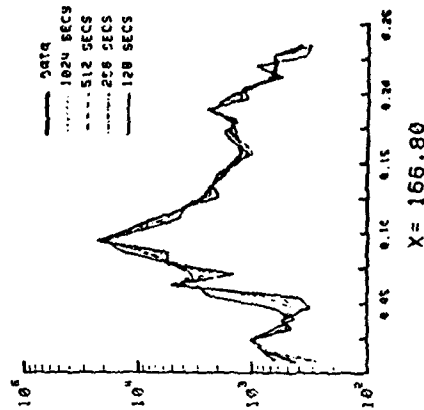
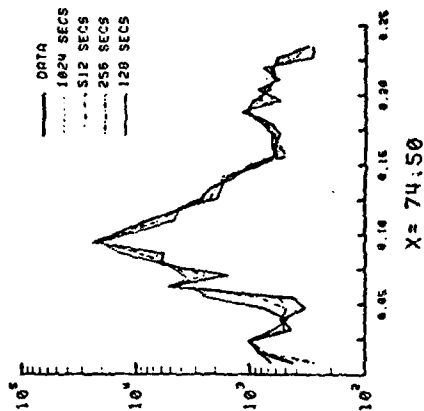
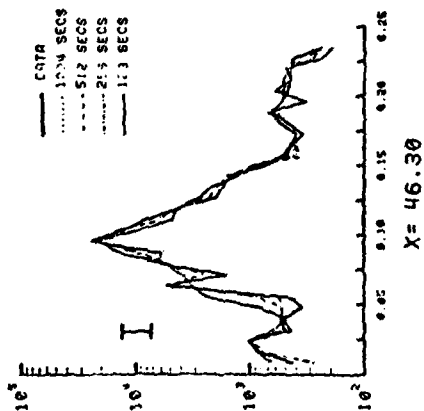
As the model (23) predicts actual time series or Fourier coefficients, not just averaged spectral quantities, it is reasonable to examine the correlation between time series predicted by the model, and those obtained from the data. In the frequency domain, such information is contained in the coherence and phase spectra (Jenkins and Watts (1969)). If the cross spectrum $C_{pq}(x_j, f)$ between two time series p and q (with Fourier coefficients $\hat{F}_p(x_j, f)$ and $\hat{F}_q(x_j, f)$) is defined by

$$C_{pq}(x_j, f) = \hat{F}_p^* \hat{F}_q \quad (31)$$

Figure 4

"Model" power spectra. "DATA" is as in figure (3); other spectra result from averaging of model predictions $M_i(x_j, f, T)$, $T=1024, 512, 256,$ and 128 seconds.

MODEL SPECTRA (NUMERICAL EXPERIMENT)



(suitably averaged over frequencies and ensembles), then the smoothed coherence $\gamma_{pq}(x_j, f)$ is defined by

$$\gamma_{pq}(x_j, f) = \left[\frac{C_{pq}(x_j, f) C_{pq}^*(x_j, f)}{C_{pp} C_{qq}} \right]^{1/2} \quad (32)$$

$0 \leq \gamma \leq 1$ is a measure of the correlation between bandpassed time series p and q . The phase $\theta_{pq}(x_j, f)$ between the time series is defined

$$\theta_{pq}(x_j, f) = \tan^{-1} \left[\frac{\text{Im}(C_{pq})}{\text{Re}(C_{pq})} \right] \quad (33)$$

If phases θ_{pq} are positive, then series p leads series q . Jenkins and Watts (1969) present approximate confidence limits for coherence and phase estimates (although, for low coherence, the confidence limits on phase become meaningless). Confidence limits are a function of the stability (equivalent dof) of the cross spectral estimates and the true coherence between the time series, but are independent of phase.

Figure (5) presents smoothed coherence spectra between model time series $M_i(x_j, t, T)$ and sampled data $S_i(x_j, t, T)$ at the six on-offshore locations shown in figures (3) and (4) for values of $T=1024$, 512, and 256 seconds. An overall degradation of coherence between model predictions and data is observed as sampled record length T decreases. In all cases, coherence is high in the frequency band 0.075-0.012 Hz, corresponding to the maximum energy portion of the power spectrum, and coherences are nearly an order of magnitude larger than would be expected if $M_i(x_j, t, T)$ and $S_i(x_j, t, T)$ were independent time series. The phase spectra shown in figure (6), independent of

Figure 5

Spectra of coherence between model predictions $M_i(x_j, f, T)$ and sampled data $S_i(x_j, f, t)$ at 6 locations x_j , $j=2-7$, for $T= 1024, 512,$ and 256 seconds. Averaged bandwidth is 0.0078 Hz. The ordinate on all plots is frequency (Hz), while the abscissa is coherence (NOT coherence²). All plots have the equivalent of 64 dof.

COHERENCES (NUMERICAL EXPERIMENT)

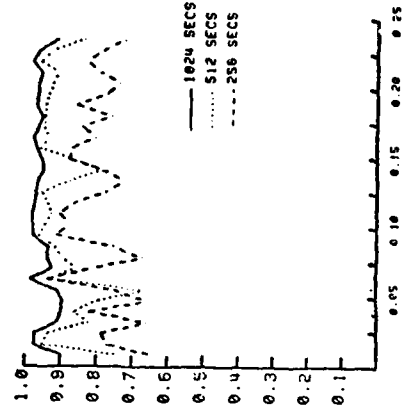
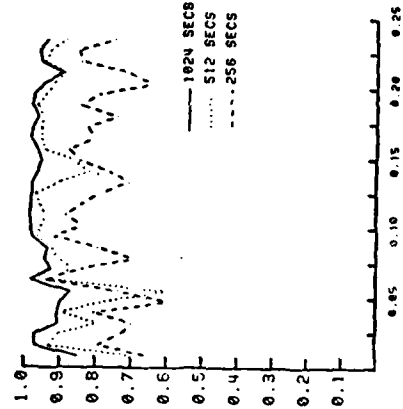
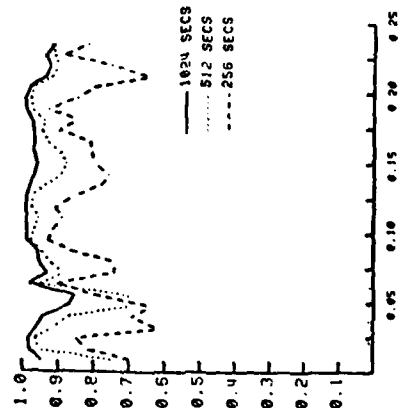
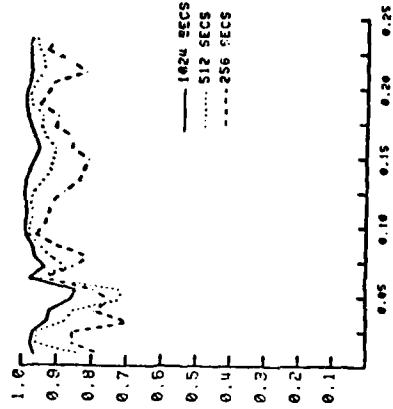
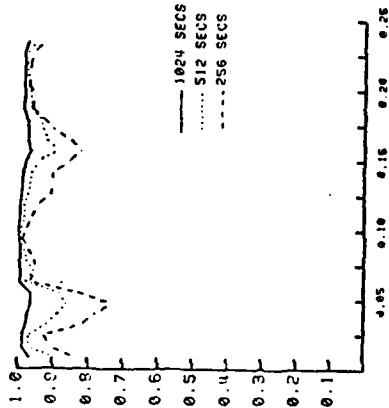
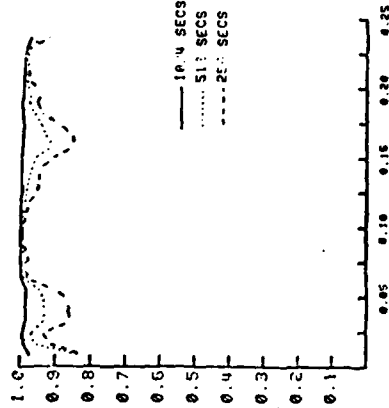
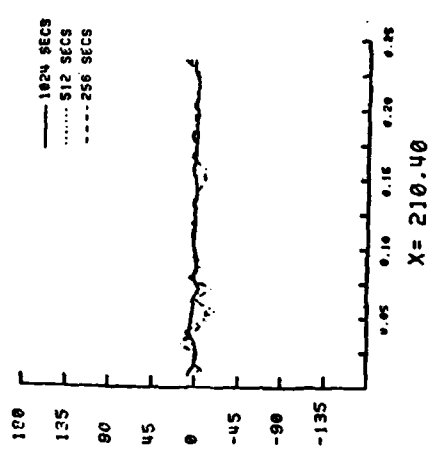
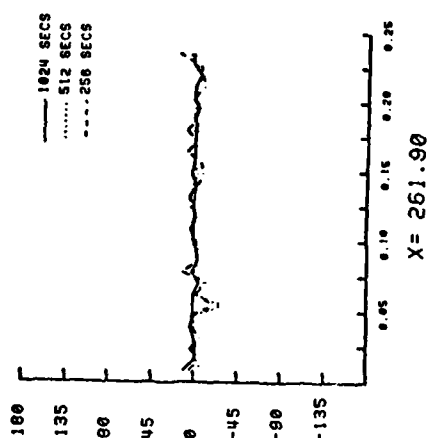
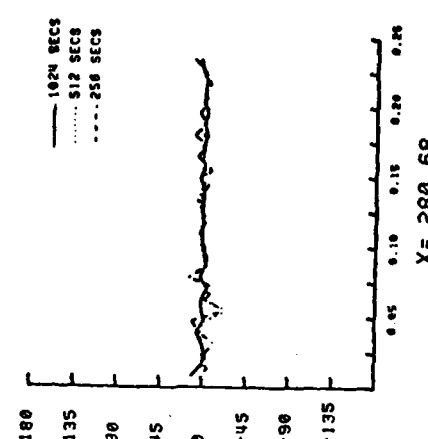
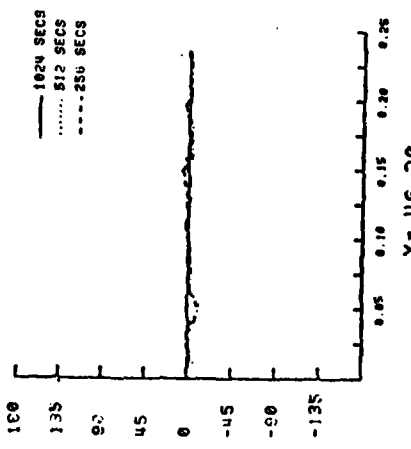
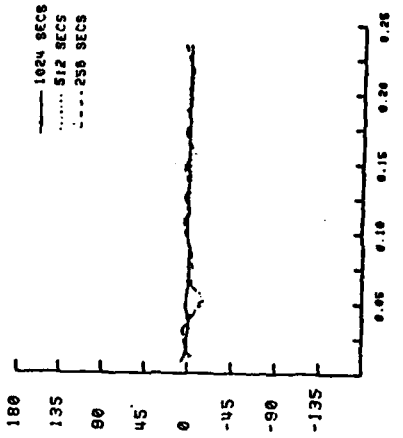
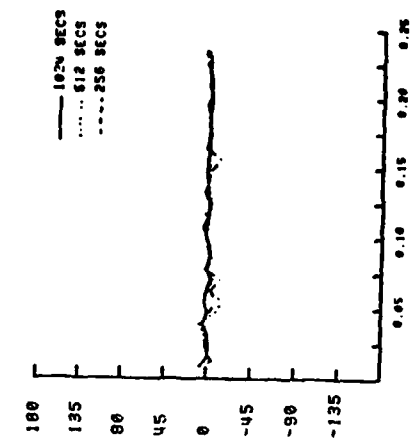


Figure 6

Spectra of relative phase between model predictions $M_i(x_j, f, T)$ and sampled data $S_i(x_j, f, T)$ at 6 locations x_j , $j=2-7$, for $T=1024$, 512, and 256 seconds. Averaged bandwidth is 0.0078 Hz. The ordinate on all plots is frequency (Hz), while the abscissa is relative phase (in degrees). All plots have the equivalent of 64 dof. A positive phase indicates that M leads S.

PHASES (NUMERICAL EXPERIMENT)



record length T , position x_j , and frequency, are consistent with zero phase lag to within 95% confidence limits (not shown).

Thus, as with smoothed spectral predictions, the model (23) is relatively insensitive to the number of modes used to represent the wave field with respect to coherence and phase between model time series and "data." The frequency and ensemble averaging used to stabilize power, coherence, and phase estimates is not strictly applicable if the true process is known a priori to be deterministic. However, as the concepts of "stochastic" and "deterministic" are properly defined only for infinite length time series, and as it is further known that the finite length outputs of some clearly deterministic systems of equations can be viewed as realizations of a stochastic process, it is reasonable, in the case of models (30) and (23), to treat both model predictions and data as realizations of stochastic processes.

In the following analysis, the deterministic models (30) and (23) will be used to predict various finite statistics of the surface gravity wave field in the shoaling region. Inputs to the models, such as the number of modes, their frequencies, initial amplitudes, and initial phases, will be obtained from data in arbitrary ways. In all cases, the time series derivable from model outputs will not be identical, to experimental precision, with measured data. On an absolute scale, therefore, the models are incorrect. We have suggested, however, that for some statistical quantities such as power, coherence, and phase spectra, the model predictions are not significantly sensitive to input conditions such as the number of

modes used to describe the wave field. In addition, it appears that the time series analysis techniques used are not operationally sensitive to the deterministic or stochastic nature of the time series on which they operate, either data time series or those derived from model outputs. Differences between the outputs of the various models and data can thus be discussed in terms of the deterministic "physics" contained (or lacking) in the models.

The Data

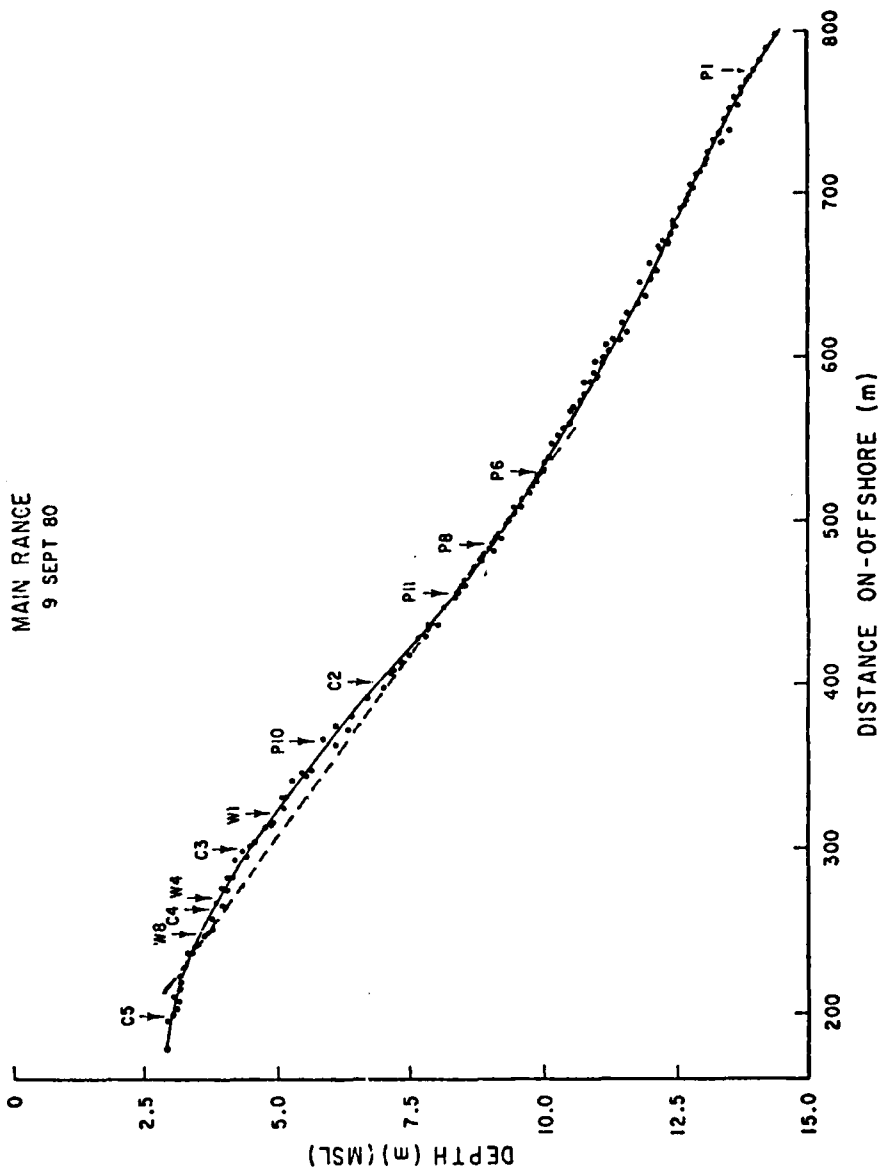
Three selected field-data sets have been compared to predictions of the model. The three sets encompass a wide range of wave energies and spectral shapes. For each data set, time series from the on-offshore sensors P1, P6, P8, P11, P10, W1, W4, and W8 were broken up into consecutive records of 1024 seconds duration. These records were then Fourier transformed and, where appropriate, Fourier coefficients of near-bottom pressure were converted to coefficients of sea-surface elevation (SSE) using the linear, finite-depth transformation (Guza and Thornton (1980)). 240 modes evenly spaced in the frequency band 0.001 - 0.234 Hz were used to represent the wave field through the shoaling region. The Fourier coefficients of SSE obtained from sensor P6 in approximately 10 m depth provided initial modal amplitudes and phases of depth-averaged velocity using the appropriate linear transformation (28.a) or (14.a). Although this procedure introduces small errors into the initial conditions, it can be shown that these errors cannot significantly affect the evolution of the wave field over distances comparable to the shoaling region.

As in the numerical experiment described previously, these initial conditions were integrated numerically to produce model predictions of Fourier coefficients at the six onshore positions corresponding to sensor locations. Although detailed measurements of bottom topography were available, the numerical integrations were carried out with assumed constant bottom slope of 2.2%. The initial depth was obtained directly from the mean pressure at P6 over the record, and thus varies in accordance with the tides. The assumed linear depth dependence on on-offshore position allows calculation of the spatial phase $\psi_n(x)$ in closed form for both models (30) and (23), thus greatly simplifying the numerical integrations. As the coupling coefficients and dispersion relations in (30) and (23) contain only weak depth dependence, and as the beach of interest is in reality nearly plane, it is not expected that the results will differ significantly from those obtained by using real topography in the integrations. Figure (7) depicts the measured on-offshore topography along the main range of instruments. It also shows the plane topography used in the integrations as well as sensor positions.

Fourier coefficients of SSE obtained directly from the data and from model integrations were then compared in a manner similar to the numerical experiment, that is, averaged spectra of SSE, coherence and phase between models and data are shown at various on-offshore locations. For the three data sets analyzed here, the wave field was found to be stationary as determined by χ^2 testing of unsmoothed spectral estimates (Haubrich (1965)).

Figure 7

On-offshore bathymetry and sensor locations along the main instrument transect. The dashed line represents the plane beach with slope 0.022 used in model integrations. On-offshore distance (in meters) is relative to an arbitrary benchmark.



5 Sept 80

The 5 Sept data set consists of 11 records (11264 seconds) obtained on a mildly rising tide. It is typical of low energy, (93 cm^2 variance measured in 10 m depth), broad-banded (in frequency) wave conditions common throughout the summer. Figure (8) presents averaged spectra of SSE calculated from the data at the four locations P1, P6, W1, and W8. The spectrum is basically flat from approximately 0.125 - 0.25 Hz, with two narrow, but not very energetic, low frequency peaks centered at 0.053 Hz and 0.077 Hz.

The spectra measured at locations P1 (14 m depth) and P6 (10 m depth) are virtually identical. This is as expected since linear shoaling effects are negligible and near resonant triad interactions are small due to the large mismatch terms in this rather deep water. From approximately 0.15-0.25 Hz, the spectra exhibit no significant differences through the shoaling region. From 0.05-0.15 Hz, the lowest frequency range with significant wind wave energy, spectral shape does not change appreciably through the shoaling region. However, there is a smooth, mild increase in spectral density with decreasing depth.

Figure (9) presents comparisons between data and model averaged spectra of SSE at six on-offshore locations. At each location, spectra obtained from the data, model (30) (labelled "BOUSS"), model (23) (labelled "CON SIS") and linear, finite-depth theory (LFDT) (labelled "LINEAR") have been plotted. Each spectrum has 160 dof, and the 90% confidence limits are shown. At all locations through the shoaling region, LFDT accurately models the

Figure 8

Averaged power spectra of SSE measured at 4 on-offshore locations. Averaged bandwidth is 0.0039 Hz. Location names, mean depth (meters) and mean variance of SSE (cm^2) are shown.

5 SEPT 80

DEPTH	VAR.
13.98	83
9.69	90
4.69	97
3.50	118

—	P1
---	P6
---	M1
---	M8

88	D0F
4	BOUND RYGD
10	-START RECORD
20	-END RECORD

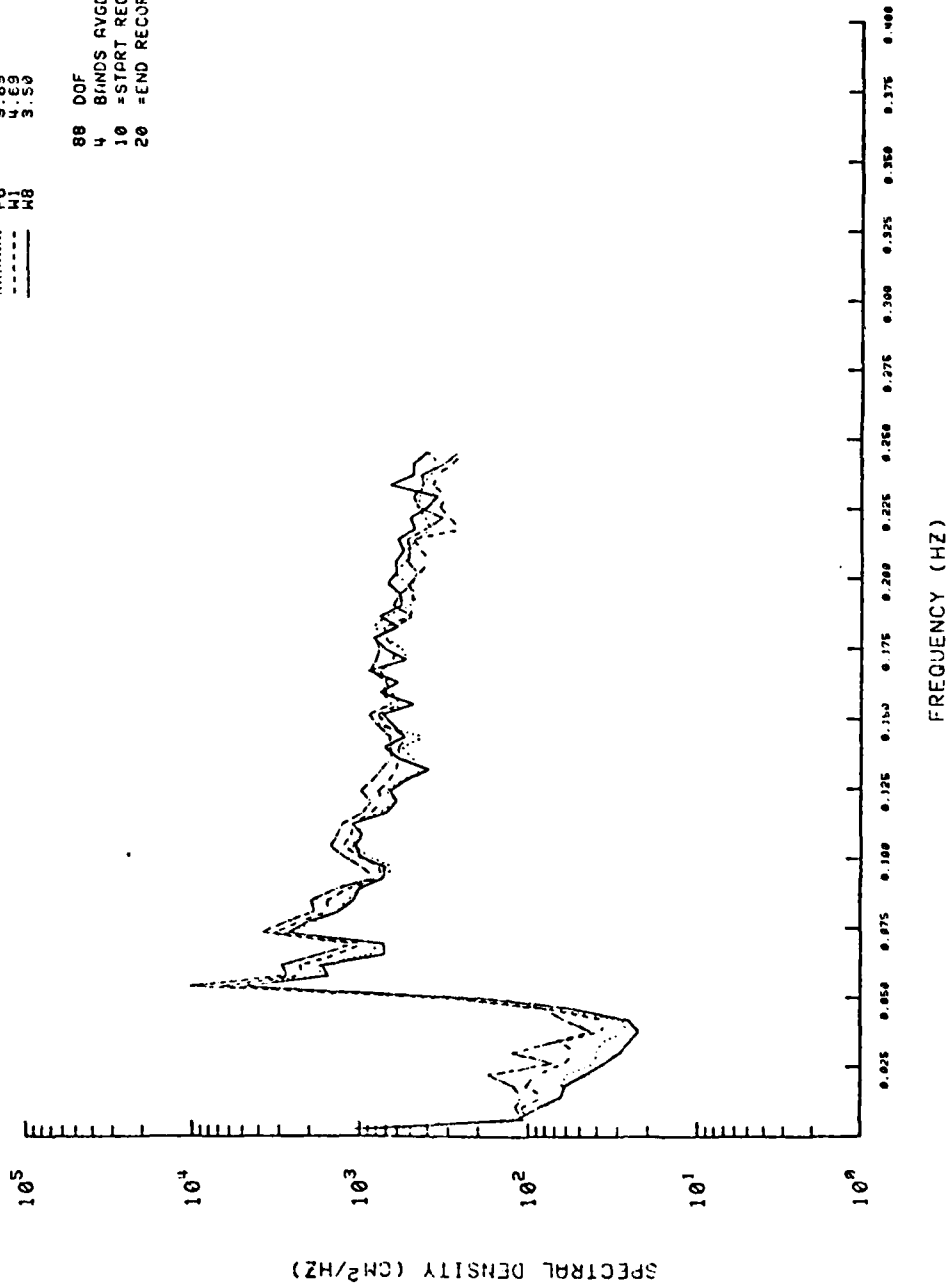
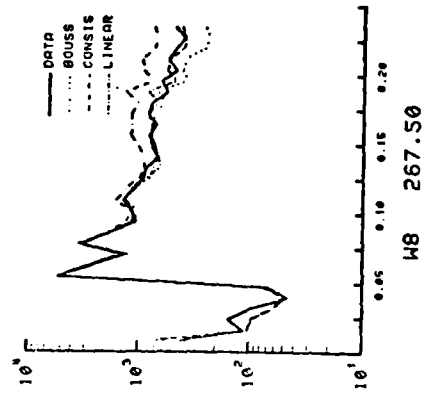
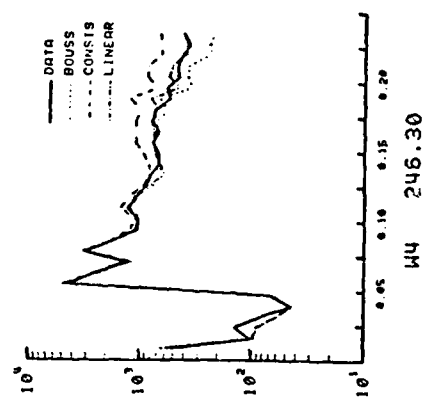
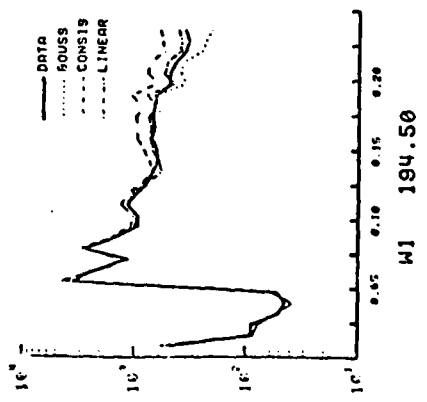
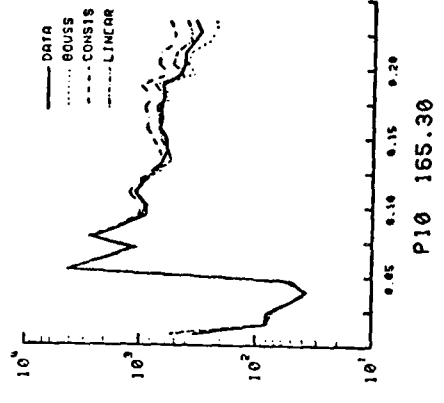
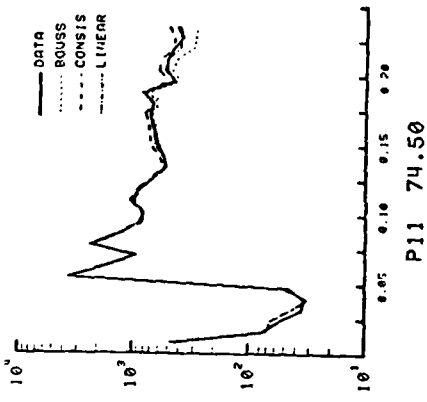
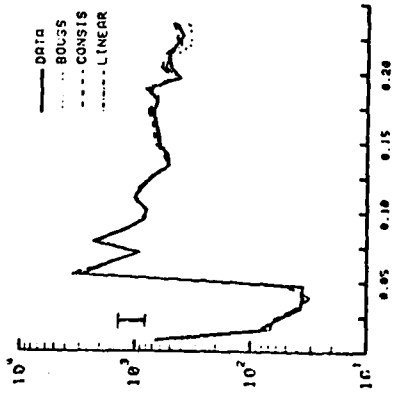


Figure 9

Comparison of averaged power spectra of SSE between measured data ("DATA"), the model (30) ("BOUSS"), the model (23) ("CONISIS"), and linear, finite-depth theory ("LINEAR"). Averaged bandwidth is 0.0078 Hz. All model input conditions were derived from data measured at P6. Shown under each plot is the location name and its on-offshore distance from the initial conditions. The ordinate is frequency (Hz) and the abscissa is spectral density (cm^2/Hz). Spectra have the equivalent of 160 dof and the 90% confidence limit is shown on the plot for P8.

5 SEPT 80 (SPECTRA)



observed spectrum of SSE. The model (30) is slightly worse only at frequencies greater than 0.18 Hz, where the model consistently underpredicts spectral density. These results are in contrast with model (23), which overpredicts spectral density in a wide frequency band from 0.12 - 0.24 Hz.

Additional information can be obtained by comparing coherence and phase spectra between the nonlinear models, LFDT, and the data. Figure (10) presents smoothed coherence spectra through the shoaling region. For both LFDT and the nonlinear models, coherence is greater than 0.9 throughout the low frequency region of the spectrum (0.05-0.10 Hz). At higher frequencies, the dominant feature of the coherency spectrum is a pronounced decrease in coherence with increasing frequency. Such a feature, which is present to some extent in all the data analyzed to date, is consistent with finite directional spread of the wave field. Model testing was carried out assuming a constant depth shoaling region and a wave field obeying LFDT. Directional spectra $E(\sigma, \theta)$ were obtained from a Maximum Likelihood (MLE) analysis of data from the shallow array of wavestaffs W2-W7. Briefly, the cross spectrum at lag r in the on-offshore can be determined if the wave field is homogeneous and the directional spectrum $E(\sigma, \theta)$ is known:

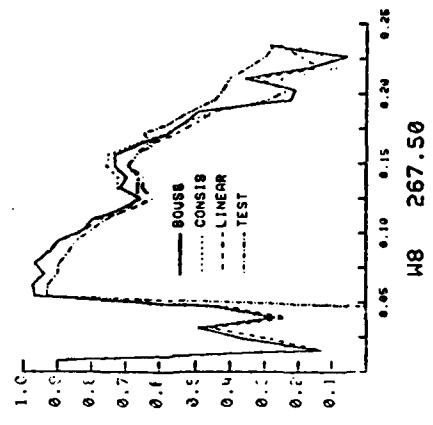
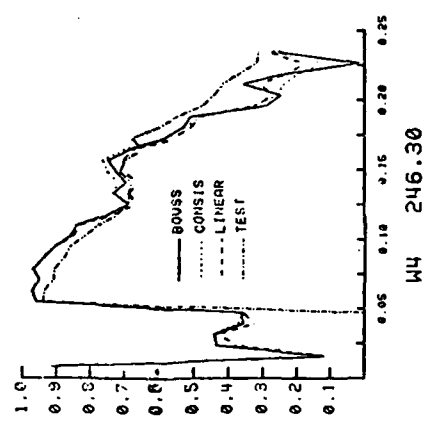
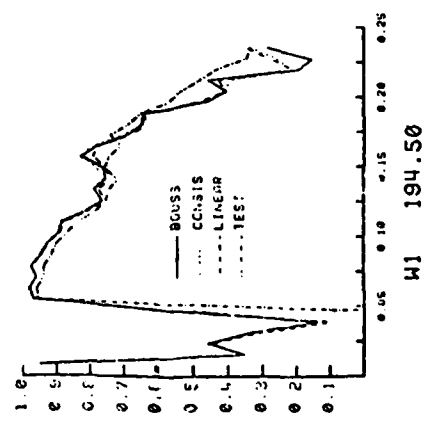
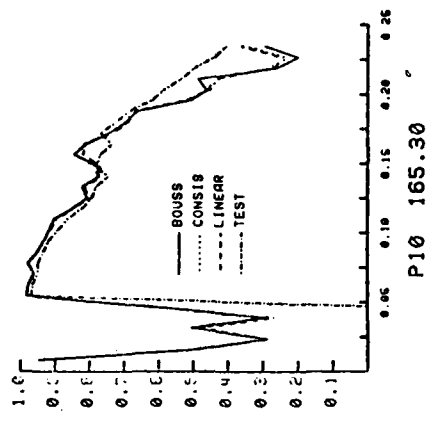
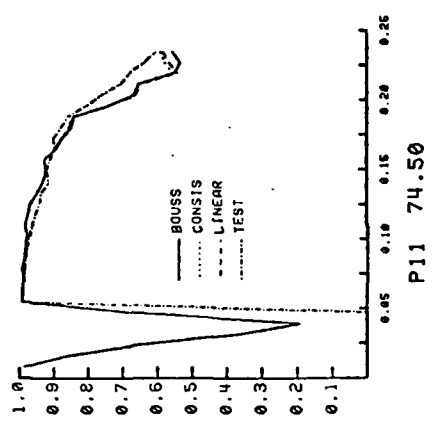
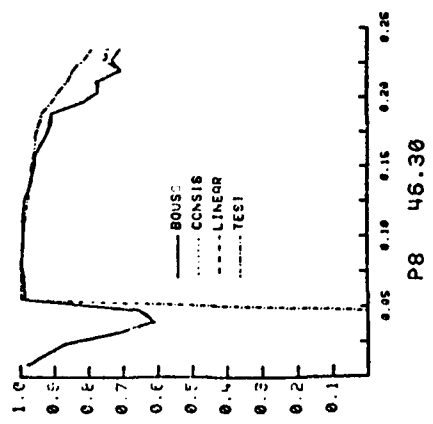
$$C(r) = \int E(\sigma, \theta) e^{ikr \cos(\theta)} d\theta \quad (34)$$

(Cartwright (2962)). Using the definition (32) of coherence and calculating the integral in (34) numerically, test coherence spectra (labelled "TEST" in figure (10)) can be generated. The general shape of the test coherence spectrum is neither a strong function of the

Figure 10

Comparison of smoothed coherence between models (30) ("BOUSS"), (23) ("CON SIS"), and linear, finite-depth theory ("LINEAR") at the 6 on-offshore locations of figure (9). Also shown ("TEST") is the coherence obtained by assuming a uniform, 5 m depth shoaling region and linear waves with the measured directional spectrum obtained from the array W1-W2-W3-W4-W5-W6-W7. Test coherences were only calculated in the band 0.05-0.25 Hz. The ordinate is frequency (Hz) and the abscissa is coherence (NOT coherence²).

5 SEPT 80 (COHERENCES)



assumed depth nor of the detailed fine structure of the directional spectrum estimates.

The shapes of the test coherence spectra are quite similar to the model-data coherences, even including the slight plateau at approximately 0.15 Hz. The dramatic falloff of the coherence spectrum with increasing frequency and distance can thus be attributed to the effects of increased directional spread in the higher frequencies, and the fact that a given spatial lag represents a larger normalized (by wavelength) lag for higher frequency waves than for lower frequencies. Additional model testing with "top-hat" directional spectra indicates that the second effect is dominant.

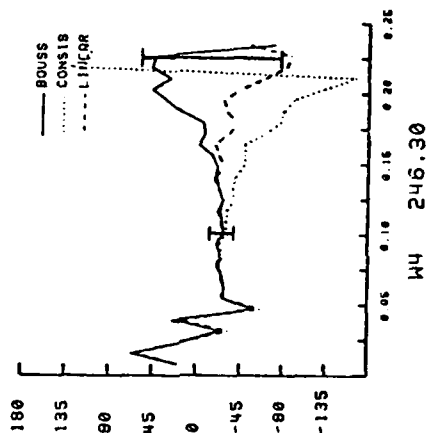
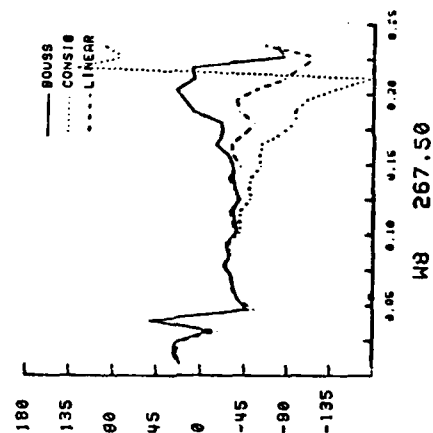
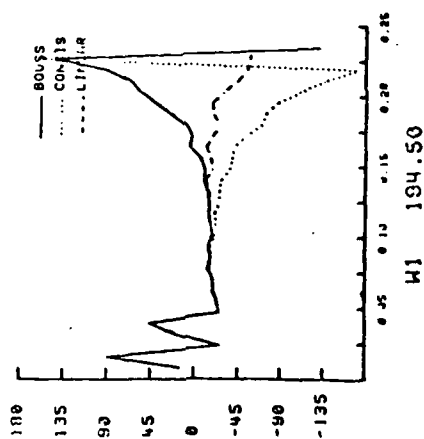
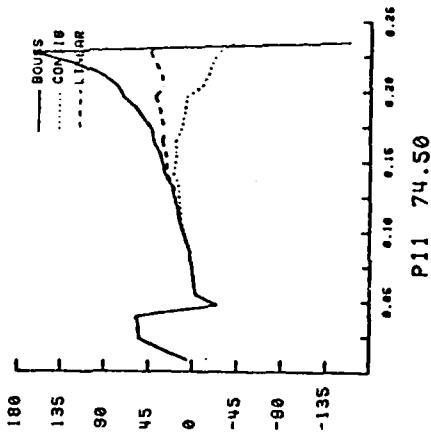
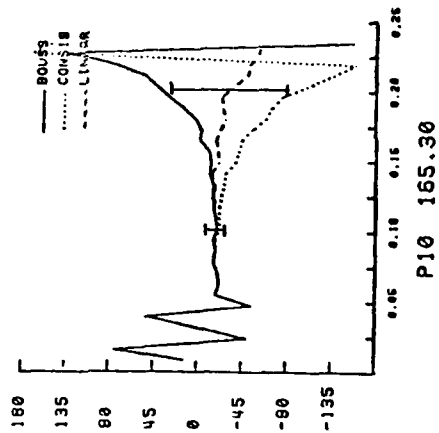
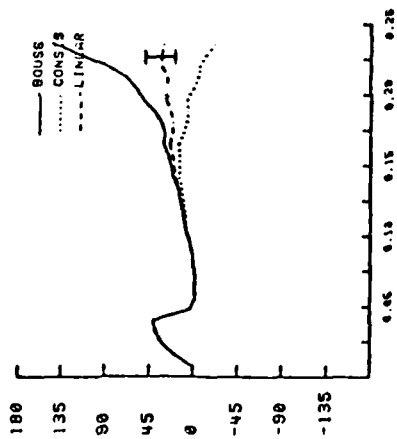
There are no significant deviations in coherence between any of the shoaling models tested. The good agreement for spectral and coherence predictions between linear and nonlinear models and the data strongly indicate that net nonlinear effects are small through the shoaling region for this particular data set. The phase spectra, presented in figure (11), can thus be interpreted for this data set in terms of the linear dispersion relations appropriate to the models (30), (23), and LFDT. It should be born in mind throughout the phase discussion that confidence limits on phase are dependent on the coherence, and thus phase estimates at the higher frequencies at the shallower reaches of the shoaling region are extremely uncertain. As the coherences for all models are virtually identical everywhere, confidence limits for all phase estimates at various frequencies have been indicated on figure (11).

LFDT phases at locations P8 and P11 are nearly consistent with

Figure 11

Comparison of relative phase spectra between shoaling models and data. Relative phase is shown in degrees. 90% confidence limits on phase (nearly the same for all three models) are shown for various frequencies and locations.

5 SEPT 80 (PHASES)



zero phase shift at all frequencies. (The very slight trend of increasing phase with increasing frequency is possibly due to a small (0.1 meter)) uncertainty in sensor position.) Both the models (30) and (23) show large deviations from the data, especially at high frequencies. The model (30) shows a strong tendency to lead the data while (23) has a lesser tendency to lag the data, although both models agree well with the data at lower frequencies. The deviations are consistent both in sign and magnitude with differences between the linear dispersion relations (28.b), (14.b), and (2.c). In the case of model (30), the linear dispersion relation grossly overpredicts wavenumber for high frequency waves in relatively deep water, as shown in figure (12). Thus the linear contribution to total phase $\psi_n(x)$ will be larger than that predicted by LFDT, and the model will lead the LFDT prediction. The second order linear phase change term, as well as the linear dispersion relation, must be taken into account for model (23). However, the magnitude of the linear phase change term is insufficient to offset the dispersion relation's underprediction of wavenumber at high frequencies in deep water (figure (12)), and thus the observed lag of the model in relation to LFDT (and hence, in this case, the data).

11 Sept 80

The second data set consists of 20480 seconds of data obtained on 11 September 1980, over a tidal maximum. With total variance in 10 m depth of over 500 cm^2 , this data set is the most energetic analyzed for this work. As seen in figure (13), the vast majority of the

AD-A111 418

SCRIPPS INSTITUTION OF OCEANOGRAPHY LA JOLLA CA SHOR--ETC F/6 8/3
RESONANCE EFFECTS ON SHOALING SURFACE GRAVITY WAVES. (U)
1982 M H FREILICH N00014-75-C-0300

UNCLASSIFIED

NL

2
1

2

END

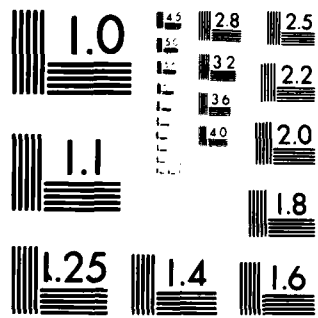
DATE

FORMED

13-82

DTIC

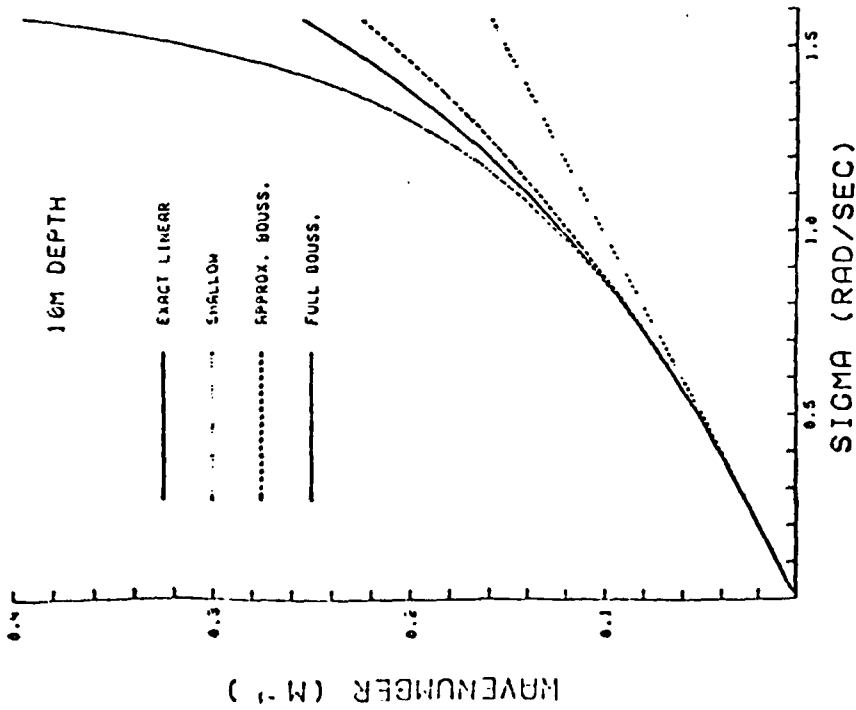
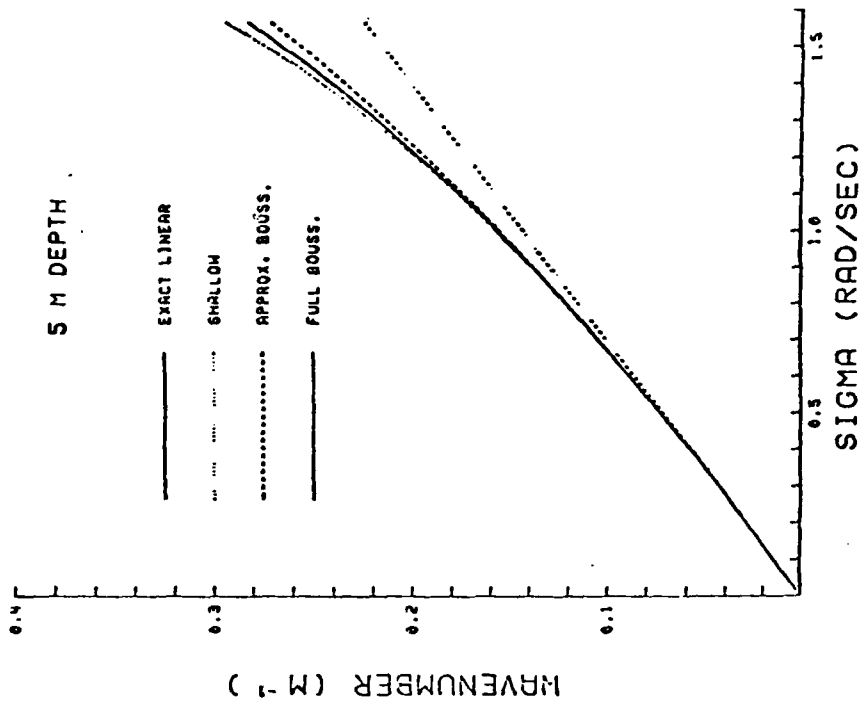
1114.15



MICROCOPY RESOLUTION TEST CHART
NATIONAL BUREAU OF STANDARDS 1963-A

Figure 12

Wavenumber vs. frequency for four linear dispersion relations at two depths, 10 m (a) and 5 m (b). The "exact Boussinesq" is equation (28.b), "approximate Boussinesq" is effective total linear wavenumber for model (23), "Linear exact" is LFDT, and "Shallow" is nondispersive shallow-water theory.



energy in the wave field at depths greater than about 10 m is concentrated in a narrow (0.016 Hz wide) band centered at 0.065 Hz. Chapter V contains a discussion of the frequency-directional characteristics of this data set. This data set is representative of long period, well-directed swell impinging on the beach. Figure (13) shows that significant spectral evolution occurs as the waves propagate shoreward through the shoaling region. In shallow water, a secondary (but significant) peak is observed centered at 0.127 Hz, nearly the exact second harmonic of the primary peak. As in the data set 5 Sept (figure (8)), no significant spectral evolution is observed between locations P1 in 14.5 m depth and P6 in 10.4 m depth.

Figure (14), similar to figure (9), compares averaged spectral predictions of the nonlinear models, LFDT, and the data. The smooth, steady growth of the secondary peak at 0.127 Hz is modeled almost precisely by the nonlinear models, but not at all by LFDT. As in the previous data set (5 Sept), the model (23) overpredicts spectral density in the high frequency (>0.15 Hz) regions of the spectrum, while model (30) exhibits a considerably smaller underprediction at high frequency. Except for frequencies near the secondary peak, LFDT accurately predicts spectral shape. However, LFDT overpredicts the power at the spectral peak by 10% (compared to only a 5% overprediction by model (30)). This fact lends credence to the hypothesis that the secondary peak is due to nonlinear transfers of energy from the primary low frequency peak to its second harmonic.

Coherence spectra are shown in figure (15). As in the case of the 5 Sept data set, the drop in coherence with increasing frequency

Figure 13

Measured power spectra of SSE for 11 Sept data set.
(Similar to figure (8)).

11 SEPT 80 (1)

DEPTH	VAR.
14.58	SEP
10.43	512
5.25	532
4.10	679

PI
P6
MI
MB

160 DOF
 4 ERRORS AVGD
 1 =START RECORD
 20 =END RECORD

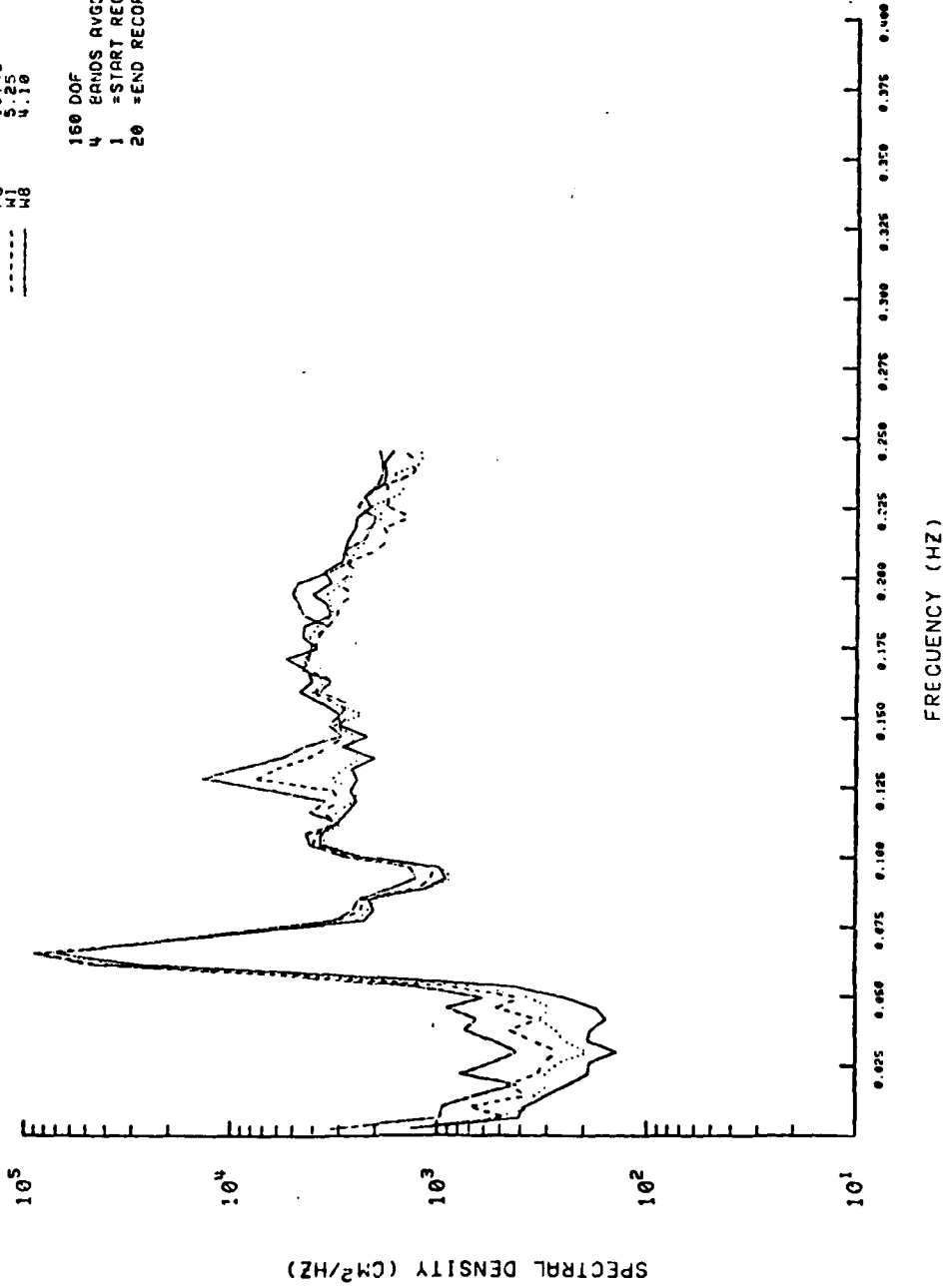


Figure 14

Comparison of averaged power spectra for 11 Sept data set. (Similar to figure (9)).

11 SEPT 80 (SPECTRA)

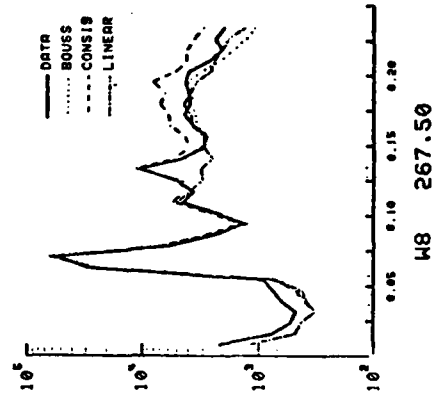
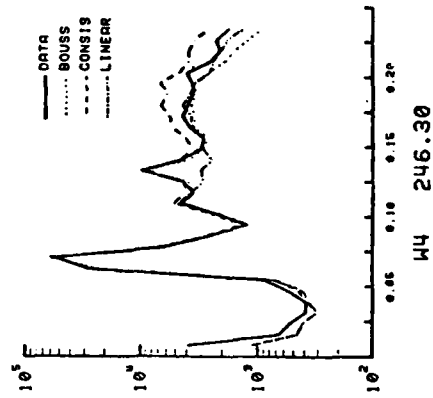
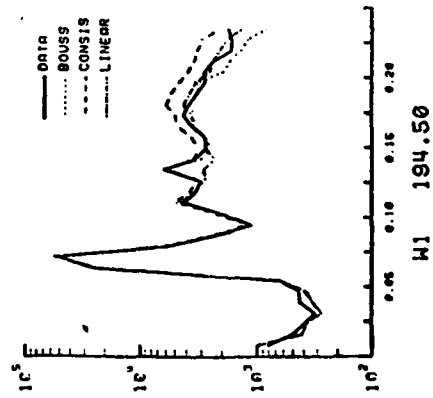
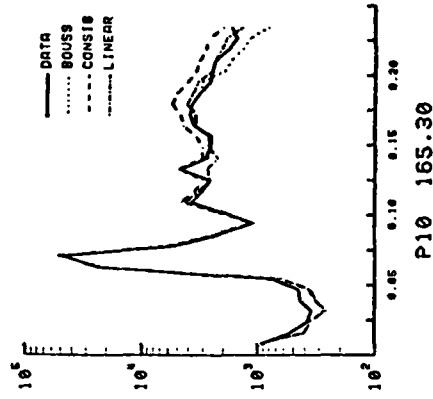
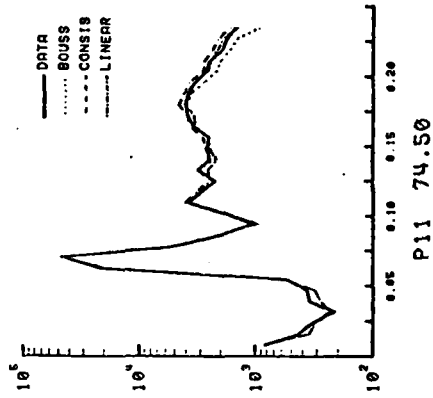
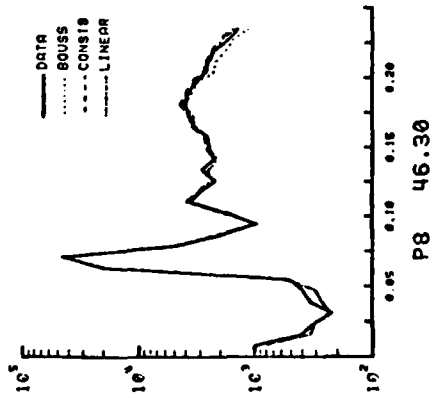
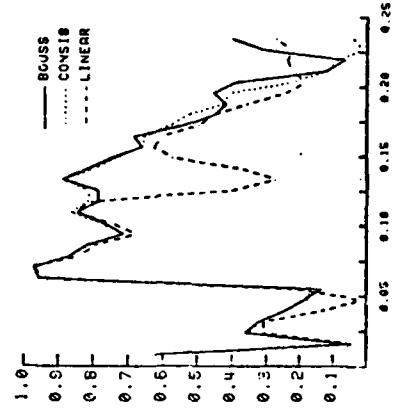
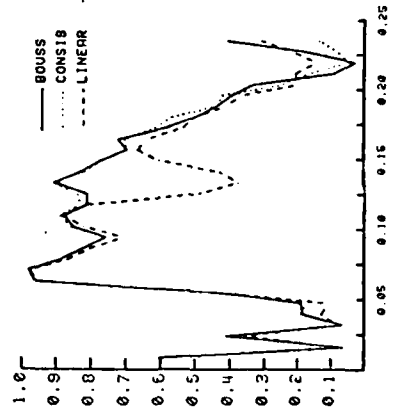
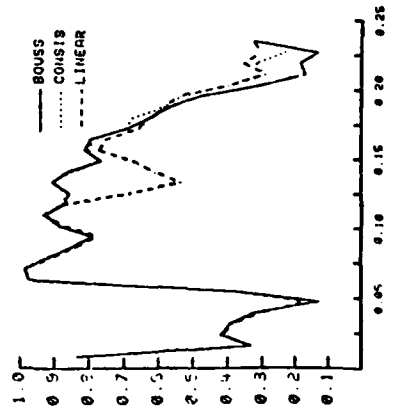
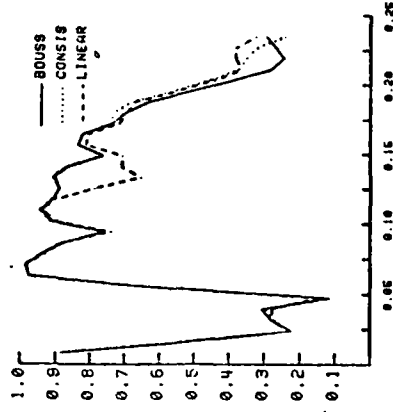
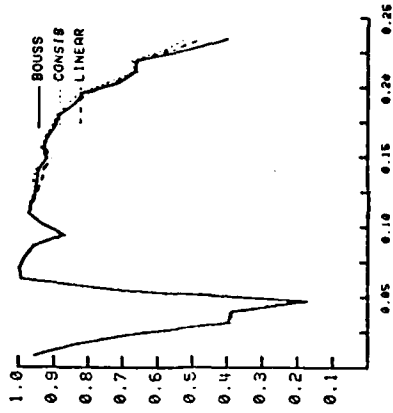
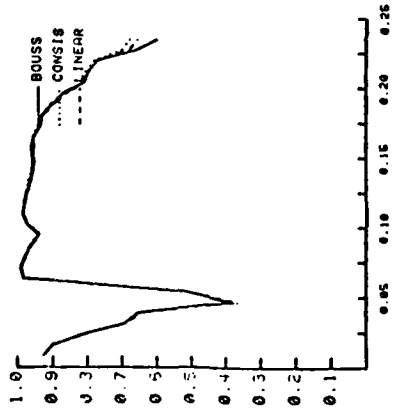


Figure 15

Smoothed coherence spectra for 11 Sept data set.
(Similar to figure (10)). Flat-bottom, directional test
coherences are not shown.

11 SEPT 80 (COHERENCES)



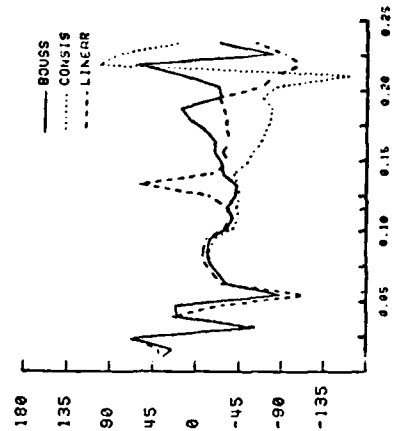
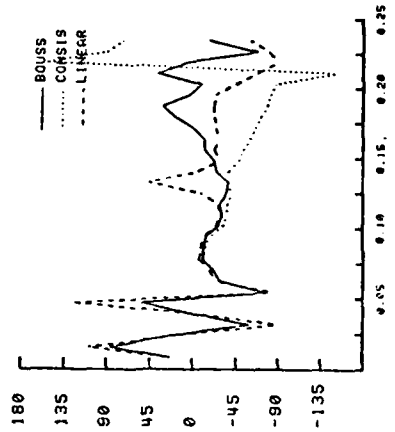
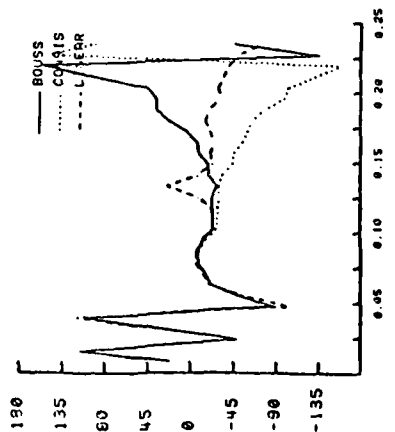
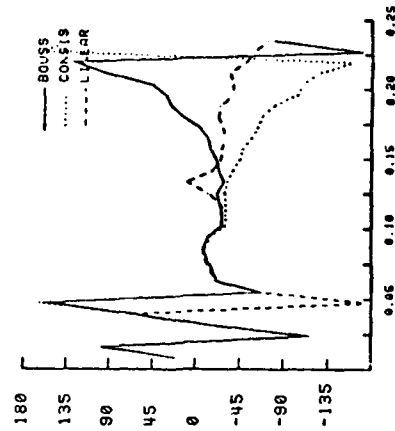
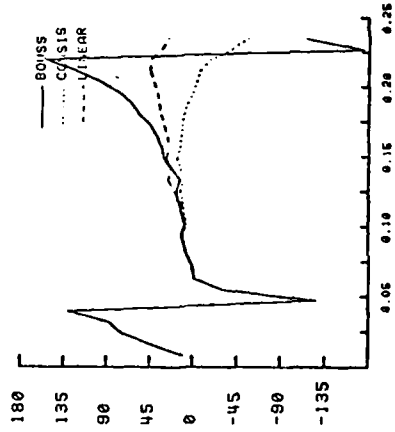
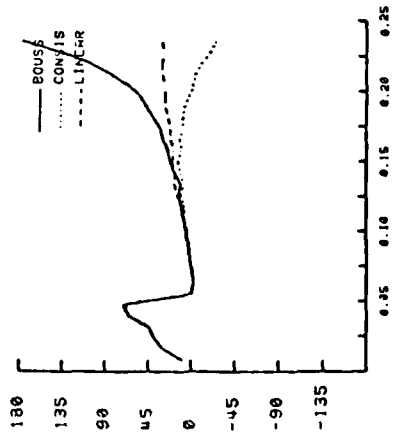
and distance from the initial point (P6) agrees well with coherence predicted by the directional spectra. In all cases the nonlinear model coherences do not differ significantly from each other, but are substantially different from LFDT at the secondary peak in the power spectrum. As the peak develops, the coherence between LFDT (which does not predict development of the secondary peak) and the data becomes progressively lower. Conversely, the coherence at 0.127 Hz between nonlinear models and the data is substantially higher on 11 Sept than it is for the 5 Sept data set (figure (10)). The drop in coherence for LFDT is restricted to the same frequency band as the secondary peak in the power spectrum; at frequencies higher and lower, there is no significant difference in coherence between linear and nonlinear models. A slight exception to this is seen at location W8, at frequencies near 0.20 Hz. A mild increase in coherence of the nonlinear models is not present in the linear model. Although the deviation between nonlinear and linear model coherences is not significant at the 95% confidence level, the fact that it occurs at the third harmonic of the primary, energetic peak in the power spectrum is indicative of nonlinear transfers of energy to the third harmonic via near resonant interactions between the primary and secondary peaks.

At locations P8 and P11, in relatively deep water where little spectral evolution is observed and coherences between all models and the data are high, the phase spectra of all models (figure (16)) are virtually identical to those of the 5 Sept data set (figure (11)). As in the discussion for 5 Sept, phase deviations can be attributed to

Figure 16

Spectra of phase between models and data for 11 Sept data set. (Similar to figure (11)).

11 SEPT 80 (PHASES)



linear dispersion differences between the models. With the exceptions of the frequency band about 0.127 Hz for LFDT and the narrow band about 0.20 Hz for the model (30), relative phases between models and data are similar to those observed in the 5 Sept data set throughout the shoaling region.

The most striking differences between data sets occurs in the frequency band about 0.13 Hz, where LFDT increasingly leads the data as one progresses through the shoaling region. It must be remembered that in this band, coherence between LFDT and the data is quite low; thus confidence intervals for phase increase, in this case, to $\pm 35^\circ$ at W8. Even considering this, the deviation is significant at all on-offshore locations. As no significant phase deviations between nonlinear models and data are observed in this band, it must be concluded that there is a nonlinearly-induced phase change in addition to the observed power spectral transfers. The change is such that the phase speed of the second harmonic is greater than that of a free, linear wave with the same frequency.

A second difference between this data set and 5 Sept is apparent near 0.20 Hz for the model (30) at the most shoreward locations W4 and W8. Rather than a smoothly increasing phase difference as would occur with waves obeying LFDT dynamics, the phase difference between model and data drops nearly to zero in this frequency band. This band is the third harmonic of the primary, and a slightly increased coherence between (30) and the data was observed as well. The phase results further confirm that nonlinear interactions, probably between the primary and the now large second harmonic, are

present in this band. Since the amplitude of the third harmonic is small, substantial phase modifications can take place (cf. equation (30.b)), and thus the actual phase in the band can be substantially coupled to the phase of the primary and second harmonic (which are predicted well by the nonlinear models), rather than the phase dictated by the linear dispersion relation.

9 Sept 80

The 9 Sept data set exhibits the most complicated evolution of any of the data so far analyzed. Composed of 17408 seconds of data obtained on a falling tide, the variance of SSE at 10 m depth (measured at 275 cm^2) falls between the low variance of 5 Sept and the high variance of 11 Sept. The power spectrum of SSE is dominated by a broad, energetic peak centered at 0.09 Hz. The high frequency ($>0.15 \text{ Hz}$) spectrum in depths greater than 10 m is flat and nearly 2 orders of magnitude down from the peak. Figure (17) shows data spectra through the shoaling region. As in the other data sets, there is no spectral evolution in depths greater than 10 m. However, through the shoaling region, the entire high frequency portion of the spectrum grows so that in 4 m depth, spectral densities are 5 - 10 times greater than in 10 m depth in the frequency band 0.15 - 0.21 Hz.

As in the 11 Sept data set, the nonlinear models accurately predict spectral evolution through the shoaling region, while LFDT does not (figure (18)). Although the model (23) appears to predict power spectral density more accurately than model (30) at frequencies greater than 0.17 Hz, the consistently large (20% - 40%)

Figure 17

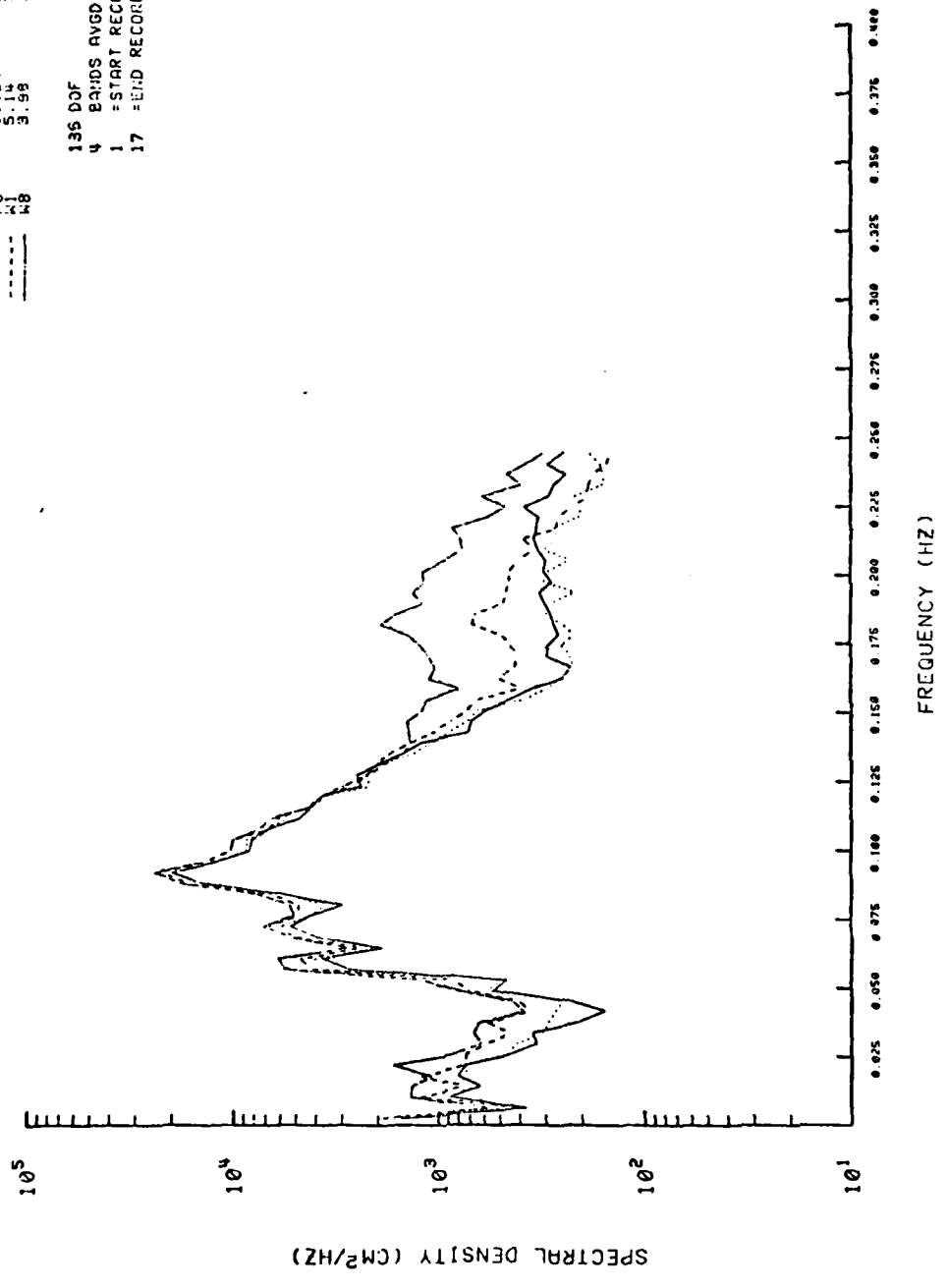
Measured power spectra of SSE for 9 Sept data set.
(Similar to figure (8)).

9 SEPT 80

DEPTH	VAR.
14.45	288
16.34	275
5.14	318
3.98	375

P1	P6	K1	K8
---	---	---	---
---	---	---	---
---	---	---	---

135 DOF
 4 BANDS AVGD
 1 -START RECORD
 17 -END RECORD

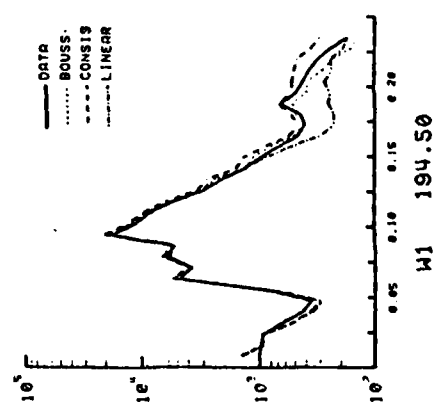
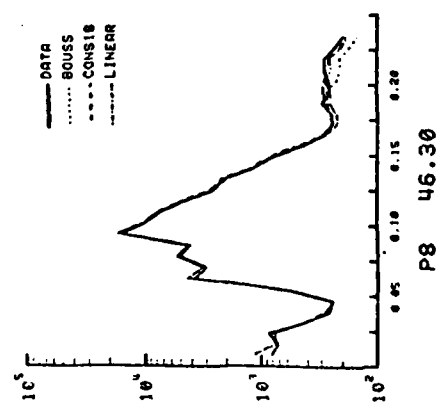
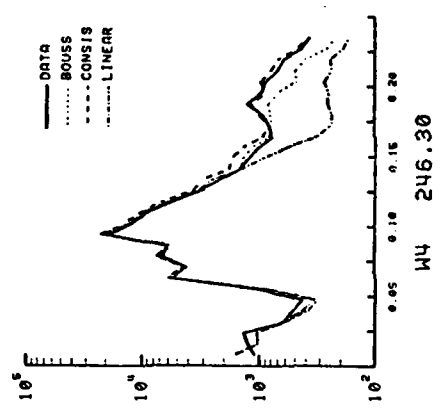
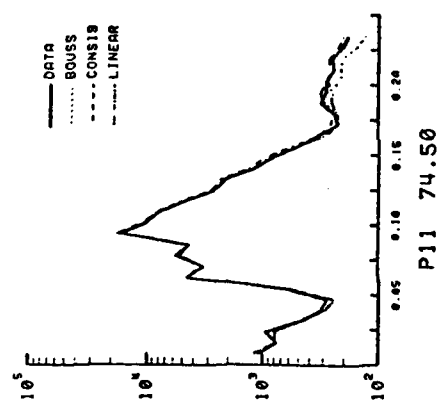
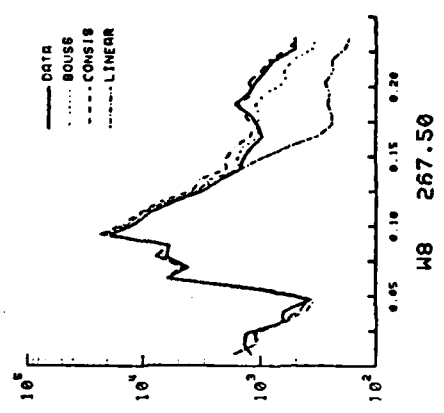
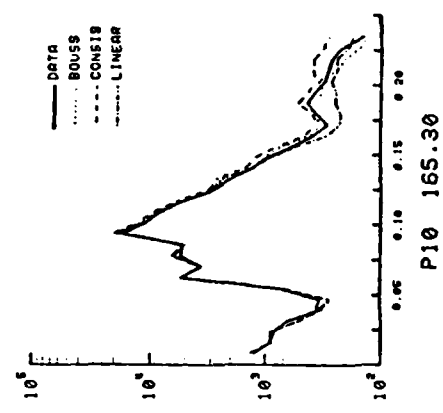


FREQUENCY (HZ)

Figure 18

Comparison of averaged power spectra for 9 Sept data set.
(Similar to figure (9)).

9 SEPT 80 (SPECTRA)



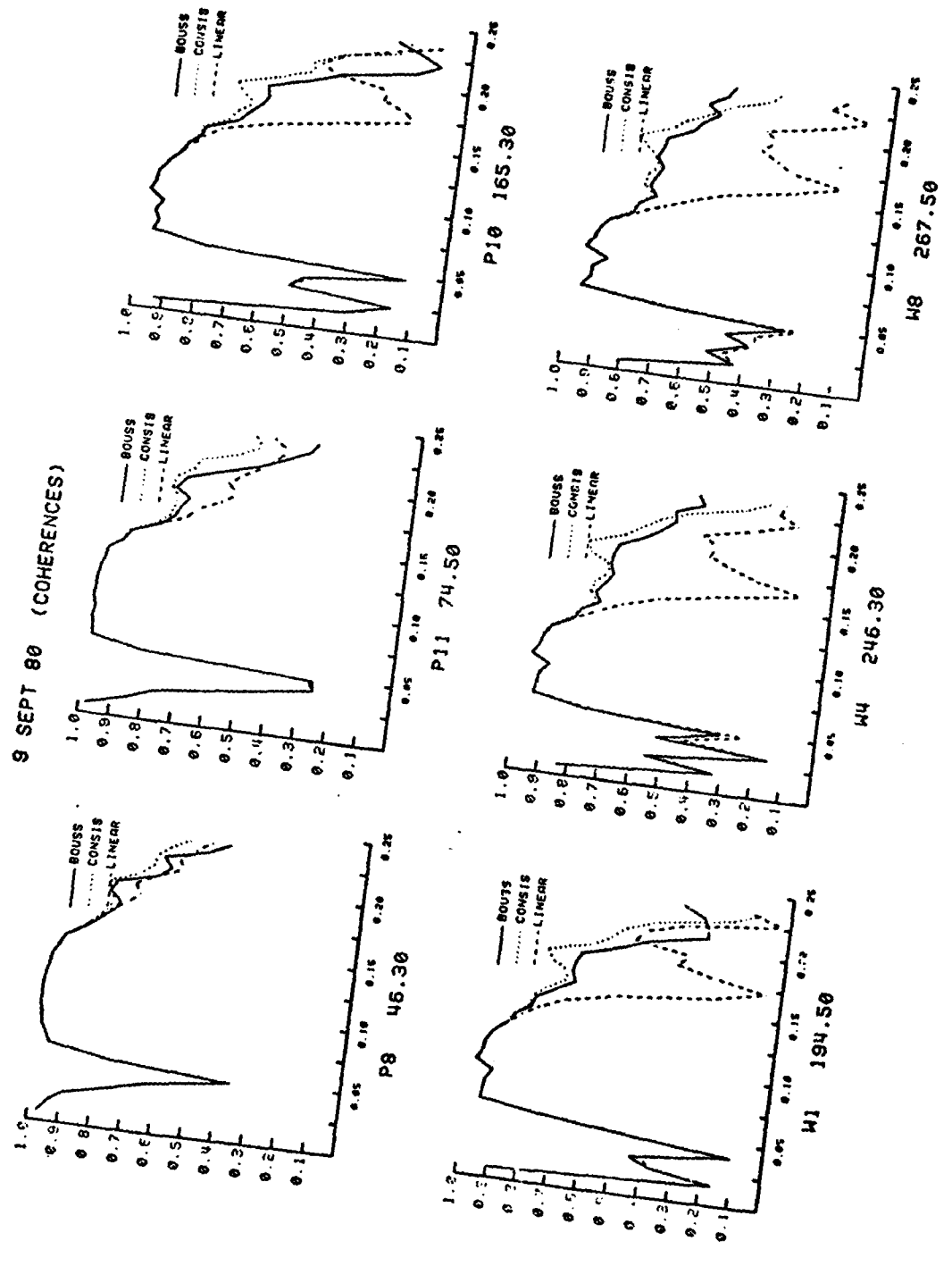
overprediction of spectral density in the band 0.09 - 0.17 Hz by model (23), not present in model (30) predictions, makes (30) a more accurate overall predictor of spectral shape. Of some interest is the fact that the evolution of the spectrum begins with the emergence of a (nonsignificant at the 90% level) peak at 0.19 Hz, the second harmonic of the highest energy portion of the broad, low frequency spectral peak. The emergence of such a structure is not unexpected, as the peak-peak-harmonic triad interaction is expected to dominate early spectral evolution due to the larger amplitudes found at the peak of the power spectrum. The importance of off-peak interactions is clear, however, as in the shallower portions of the shoaling region the entire high frequency end of the spectrum has increased significantly.

The coherence spectra shown in figure (19) are further evidence of the complicated evolution of the wave field as it propagates through the shoaling region. Apart from the barely significant coherence peak at 0.19 Hz apparent in models (30) and (23), the basic shape of all coherence spectra at locations P8 and P11 is again consistent with measured directional spectra. At all locations, all models have high coherence in the energetic region of frequency space (0.063 - 0.125 Hz). However, at locations P10 through W8, significant deviations between models are evident in the high frequencies. Coherence between LFDT and the data drops dramatically with decreasing depth, first in the band 0.13-0.20 Hz, then throughout the high frequency region. At the same time, coherence between the nonlinear models and the data actually increases significantly in the high frequency region. Such an effect is clearly not due to finite

Figure 19

Smoothed coherence spectra for 9 Sept data set. (Similar to figure (10)). Flat-bottom, directional test coherences are not shown.

9 SEPT 80 (COHERENCES)



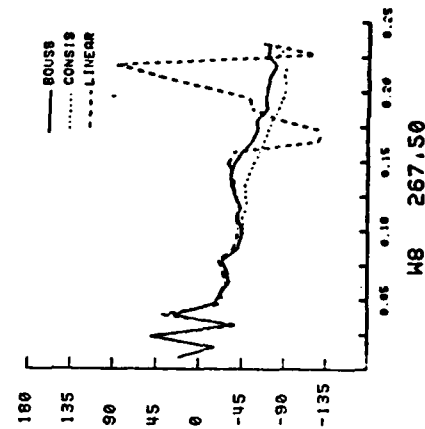
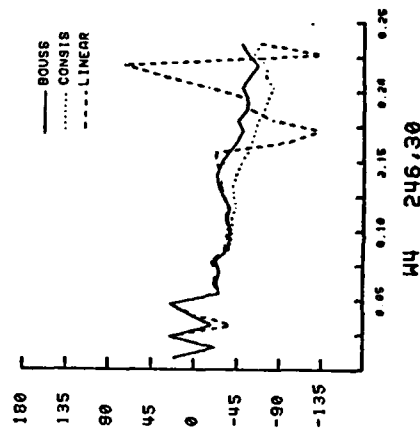
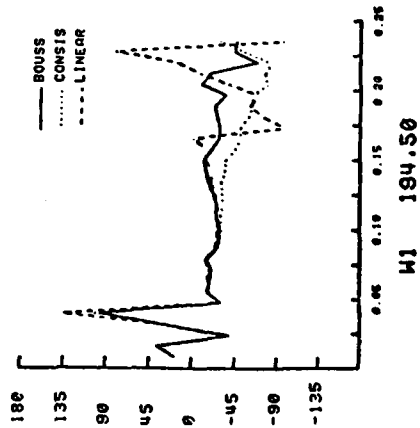
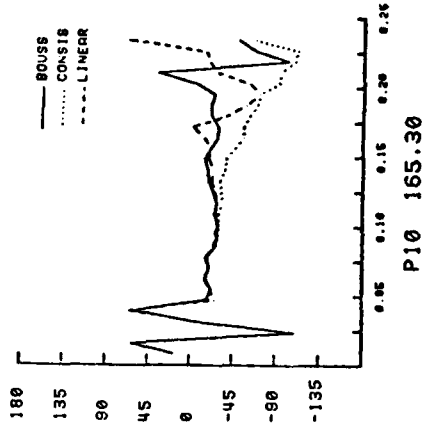
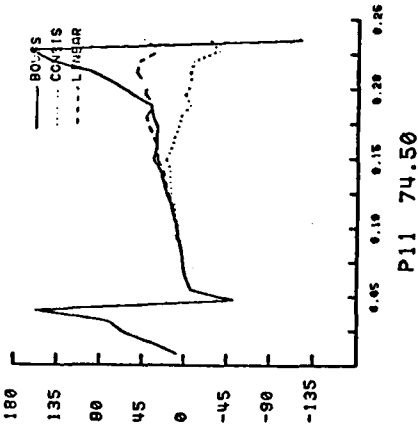
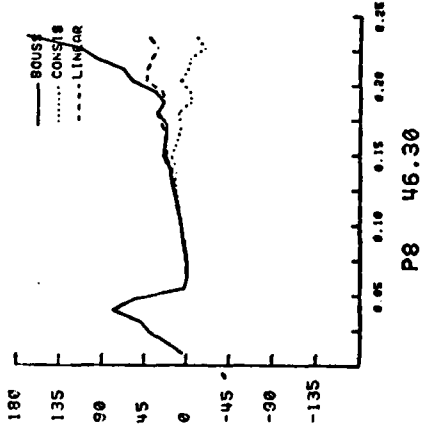
directional spread in a homogeneous, linear, wave field, but must be attributed to the fact that the high frequency wave field is dominated by nonlinear interactions with lower frequency components.

The nonlinearities are also evident in the phase spectra (figure (20)). Phases at locations P8 and P11 evolve similarly to those of previous data sets, in accordance with simple LFDT dispersion. At the shallower locations P10 through W8, the breakdown of linear dispersion is clear. The phase relationship between linear theory and the data at high frequencies is neither monotonic nor consistent with zero phase lag (although once again it must be remembered that coherence is low in this region of frequency space). In terms of phase speed, some frequency components appear to be travelling faster than predicted by LFDT, and some slower! Rather than model (30) leading the data in the high frequencies, as predicted by linear dispersion arguments and observed in the basically linear 5 Sept data set (figure (11)), the model actually lags the data slightly. The model (23) phases exhibit none of the sharp lag predicted by linear dispersion, but instead are nearly identical with phases predicted by model (30). It thus appears that nonlinear interactions, properly modeled by both (30) and (23), completely dominate the high frequency portion of the wave field in this particular data set.

Figure 20

Spectra of phase between models and data for 9 Sept data set. (Similar to figure (11)).

9 SEPT 80 (PHASES)



V. DISCUSSION AND CONCLUSIONS

The present work has developed and tested models describing the changes undergone by wind-generated surface waves (4-18 second periods) as a broad spectrum of such waves propagates shoreward over a shoaling bottom. Two, one-dimensional models based on variants of the Boussinesq equations and incorporating the physics of multiple near resonant triads have been derived and implemented numerically. The models, which assume that all waves are normally incident to the beach, have no empirically determined parameters.

A field experiment involving dense instrumentation of the shoaling region from 10 m depth to 3 m depth was successful in obtaining detailed measurements over a wide range of wave conditions. Three selected data sets spanning the range of observed wave conditions and spectral evolution have been analyzed in depth and compared with power spectra, coherence, and phase predictions of the two nonlinear shoaling models and linear, finite-depth theory.

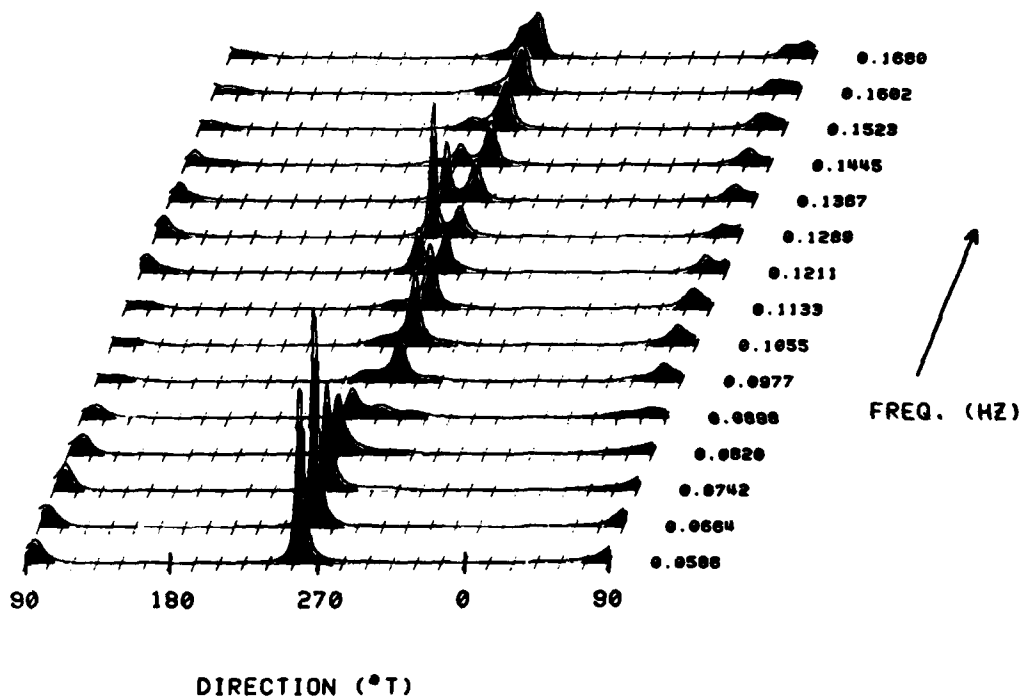
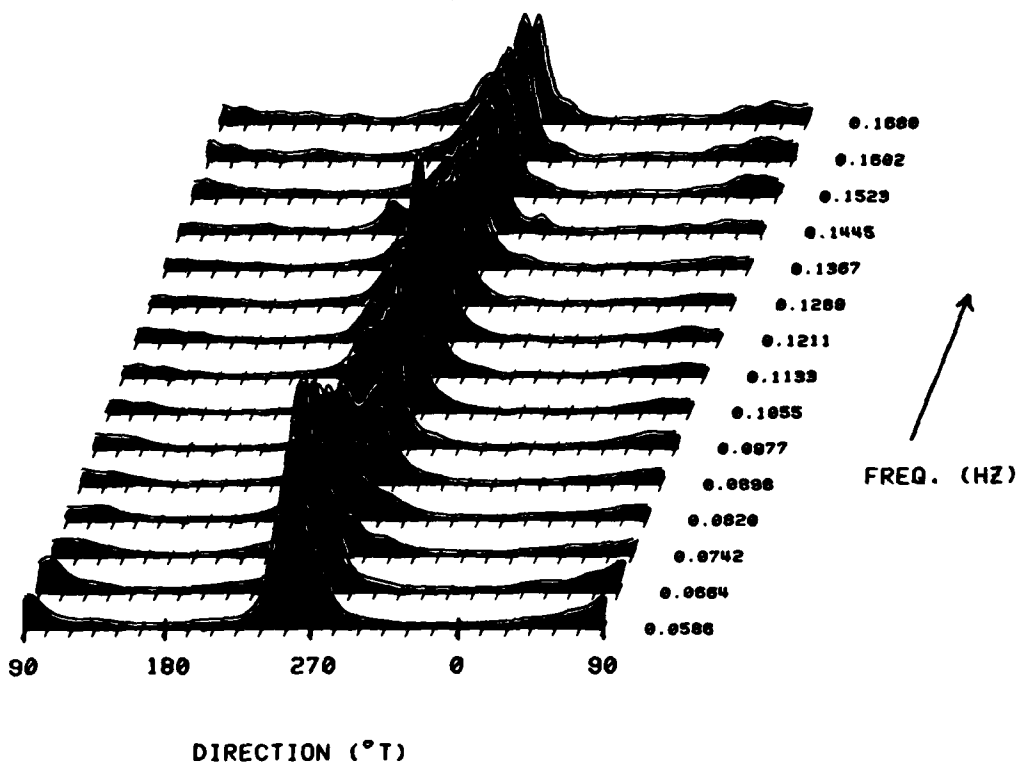
Overall, both nonlinear models were good predictors of the power spectrum of sea-surface elevation throughout the shoaling region. Linear theory was considerably less accurate except under broad-banded, low energy conditions. Coherence between predictions of all models and the data was uniformly high in the low-frequency (generally energetic) region of the wind-wave band. With the exception of those regions of space (both physical and frequency) where significant nonlinear evolution of the spectrum was taking place, the features of all model-data coherence spectra were similar and adequately accounted for by the measured directional spread of the

wave field. Where nonlinear effects were important (shallow water, mid- to high-frequencies), coherences between the nonlinear models and the data improved markedly compared to "linear" regions of the spectrum, while coherence between linear, finite-depth theory (LFDT) and the data became dramatically worse. In spatial regions where nonlinear effects are small, LFDT is an accurate predictor of phase across the entire wind-wave spectrum. In these regions, phase deviations between the nonlinear models and the data can be ascribed to differences in linear dispersion relations; the long wave assumptions inherent in the derivation of the Boussinesq-type models make them poor predictors of wavenumber for high-frequency waves in relatively deep water. Where nonlinear effects are important in the evolution of the power spectrum, the nonlinear models are good predictors of phase whereas LFDT is significantly poorer, indicating that nonlinear phase changes (which can, for instance, generate the observed asymmetrical shape of waves near breaking) are as evident as the more often documented nonlinear energy transfers.

The accurate predictions of the nonlinear shoaling models over a broad range of input wave conditions makes them especially appealing. Some specific data sets (eg. 5 Sept, figures (8) to (11)) are predicted well by LFDT. The evolution of harmonics in some data sets (eg. 11 Sept, figures (13) to (16)) is reminiscent of Stokes-type forced theories (although the similarity is merely illusory as the Ursell number in 5 m depth is greater than 1). In all cases so far observed, the more general nonlinear shoaling models (23) and (30) accurately predict the observed spectral evolution of the wave field

Figure 21

Frequency-directional spectra in the wind-wave band for the 11 Sept data set. The top spectrum is obtained from MLE analysis of the two-dimensional deep array shown in figure (2), excepting the nonfunctional current meter. The bottom spectrum results from a similar analysis of the linear shallow array of wavestaffs W2-W7. Placement inaccuracies resulted in staffs W2 and W7 being far enough shoreward and seaward (respectively) of the longshore line to allow for resolution of onshore- vs. offshore-propagating energy. Scaling is such that at any frequency, the total area under the curve is proportional to $\log(\text{spectral density})$ in that band.



through the shoaling region; in the three data sets analyzed here in depth, the models properly predict nonlinear phase evolution as well.

Directional effects appear to play little role in the nonlinear evolution of the data sets analyzed here. In part this is due to the fact that Torrey Pines Beach has few open windows to the deep ocean, and thus energetic low- and mid-frequency waves tend to have narrow, well-defined directional spectra. More generally, however, these waves refract considerably before entering the relatively shallow water of the shoaling region, and thus the extremely broad directional distributions typical of the open ocean are not expected.

Figure (21) shows two, averaged, frequency-directional spectra from the 11 Sept data set. The top figure displays data obtained from the two-dimensional deep array (see figure (2)). Note that the energy in the low-frequency peak of the power spectrum (0.065 Hz) is directed from approximately 15° south of true west, and has a width of only 25° . It is likely that this swell is being generated by a distant storm in the southern hemisphere. Pawka (1981) discusses details of the directional spectrum for similar data sets. Of interest to the present study is the fact that, although the majority of the energy at frequencies greater than 0.10 Hz is directed from the northern quadrant, approximately half of the energy at the harmonic frequency (0.127 Hz) is directed from the south, similar to the low frequency primary. The effect is enhanced in the data from the shallow array, shown in the lower half of figure (21). In general, directional spreads measured at the shallow array are narrower than at the deep

array, as expected on the basis of simple linear refraction. At the harmonic frequency band, the vast majority of the energy comes not from the north but from the south. This is expected if, as hypothesized in Chapter IV, the energy in the harmonic peak is due primarily to nonlinear transfers via peak-peak-harmonic triad interactions. As the resonance condition (15.b) is a vector equation, any peak-peak-harmonic interaction will force a harmonic wave whose wavenumber points in the direction of the peak waves.

The directional spectra also provide preliminary bounds on the amount of seaward-propagating energy in the shoaling region. Direct integration of directional spectral estimates in the frequency range 0.059-0.152 Hz for all data sets reveals that at no time is more than 25% of the total energy in any band propagating westward in the window 45° - 135° at the shallow array, and less than 20% at the deep array.

Average values of seaward-propagating energy are approximately 17% for the shallow array and 14% for the deep array. However, model testing of the MLE estimator indicates that the data-adaptive analysis technique has a tendency to window incoming energy incorrectly into outgoing directions for the arrays in this experiment. The model tests suggest that there is a strong possibility that the true amount of outgoing energy is negligible (in the range 0-10% of total energy) at frequencies in the wind-wave band. The predictions of the one-dimensional shoaling models clearly are not significantly affected by such small amounts of outgoing energy. Should a more quantitative description of seaward-propagating energy be desired, a special-purpose analysis window with minimal windowing error of incoming to

outgoing energy, similar to those discussed in Davis and Regier (1977) and Pawka (1981), should be implemented.

The role of the sloping bottom is found to be of only minor importance in determining spectral evolution of the wave field through the shoaling region. Comparison of power spectral results from the numerical experiment (figure (4)) with those from the 9 Sept data set (figure (17)) from which initial conditions for the flat-bottom numerical experiment were drawn, shows that the qualitative nature of the evolution of the spectrum is similar in both cases. Bottom slope appears explicitly only in the linear shoaling terms in (30) and (23), and implicitly in the calculation of total phase necessary to determine the trigonometric modulation of the nonlinear coupling. Differences between the linear shoaling terms, due to differences between linear dispersion relations, account for much of the deviation between power spectral predictions of models (30) and (23), and the data. This is true of all frequencies in the 5 Sept data set and at those (generally very high) frequencies in other data sets where nonlinear spectral evolution is not apparent. In a given frequency band, linear shoaling predicts that the ratio of energies at two depths (neglecting refractive effects) is inversely proportional to the ratio of group velocities (defined as $\frac{\partial \sigma}{\partial k}$) at those depths. The nondispersive form of the dispersion relation (14.b) overpredicts (in comparison to LFDT) the ratio of linear group velocities

$$C_g(\text{deep})/C_g(\text{shallow})$$

and hence overpredicts the ratio

$$E_{\text{tot}}(\text{shallow})/E_{\text{tot}}(\text{deep})$$

over most of the wind-wave band. Conversely, the Boussinesq dispersion relation (28.b) underpredicts the ratio

$$C_g(\text{deep})/C_g(\text{shallow})$$

but remains within 10% of LFDT for frequencies less than 0.17 Hz everywhere in the shoaling region. (Care must be taken when attempting to isolate the effects of individual terms in the rate equations. Since the models (30) and (23) allow weak nonlinear interactions across all frequencies, a misprediction in the evolution equations, even if confined initially to a small band of frequencies, can feed back through the nonlinear coupling to cause errors at other frequencies and other on-offshore locations.)

The observed lack of power spectral evolution between 14 m depth (P1) and 10 m depth (P6) strongly indicates that the process of triad near resonance modeled by (30) and (23) is in fact confined to the relatively shallow shoaling region. Although the models are not valid in depths much greater than 10 m due to breakdown of the long wave assumptions over much of the wind-wave frequency band, the trend toward increasing inability to satisfy the resonance conditions for triads containing high-frequency waves suggests that the triad resonance mechanism is unimportant in such relatively large depths. That this is observed in the data bodes well for future attempts to smoothly match the present model with one more appropriate to deeper water.

Finally, it should be noted that the numerical integration of highly resolved spectra is extremely time consuming and therefore (perhaps prohibitively) expensive. A typical day's data takes

approximately 100 hours to be integrated on a fast (Perkin-Elmer 8/32) minicomputer with highly optimized code. The present results, coupled with analysis of the structure of models (30) and (23), suggest some simplifications.

Clearly, for broad-banded, low energy wave conditions, weakly nonlinear resonant interactions are small compared with linear effects. As the phase comparisons on 5 Sept showed, it is advantageous to use LFDT due to its apparently more accurate dispersion relation at all frequencies through the shoaling region. Quantitative limits on "broad-banded" and "low energy" have not been established.

Narrow-banded input spectra, such as 11 Sept, tend to concentrate nonlinear effects at the harmonics of the input peak frequency. This is due to the fact that the product of amplitudes in the nonlinear term is large for triads involving two large-amplitude modes. Although the net effect of a large number of interactions with low energy modes cannot be ignored on ordering grounds, it appears that in practice large amplitude, peak-peak-harmonic interactions dominate the evolution of harmonic bands. A code in which LFDT is used to predict evolution away from the harmonic bands coupled with high resolution nonlinear evolution at the harmonics is expected to be a good predictor of the shoaling transformation. Note that the second harmonic band should be approximately twice the width of the primary band, etc. Work is currently proceeding along these lines.

REFERENCES

- Armstrong, J.A., N. Bloembergen, J. Ducuing, and P.S. Pershan, 1962, Interactions between light waves in a nonlinear dielectric, *Physical Review B*, v 127, p 1918-1939.
- Aubrey, D.G., 1978, Statistical and Dynamical Prediction of Changes in Natural Sand Beaches, PhD. Thesis, UCSD-SIO, 194 pp.
- Barber, N.F., 1961, The directional resolving power of an array of wave detectors, in *Ocean Wave Spectra*, Prentice-Hall, Englewood Cliffs, p 137-150.
- Benney, D.J. and P.G. Saffman, 1966, Nonlinear interactions of random waves in a dispersive medium, *Proc. Roy. Soc. A*, v 289, p 301-320.
- Boussinesq, J., 1871, Theorie generale des mouvements qui sont propages dans un canal rectangulaire horizontal, *C.r. Acad. Sci. Paris*, v 73, p 256-260.
- Bretherton, F.P., 1964, Resonant interactions between waves: The case of discrete oscillations, *J. Fluid Mech.*, v 20, p 457-480.
- Bryant, P.J., 1973, Periodic waves in shallow water, *J. Fluid Mech.*, v 59, p 625-644.
- Bulirsch, R. and J. Stoer, 1966, Numerical treatment of ordinary differential equations by extrapolation methods, *Numerische Math.*, v 8, p 1-13.
- Carrier, G.F. and H.P. Greenspan, 1958, Water waves of finite amplitude on a sloping beach, *J. Fluid Mech.*, v 4, p 97-109.
- Cartwright, D.E., 1962, Analysis and statistics, in *The Sea* vol. 1, Hill, ed., Interscience, New York, p 567-586.
- Chu, V.H. and C.C. Mei, 1970, On slowly varying Stokes waves, *J. Fluid Mech.*, v 41, p 873-887.
- Cole, J.D., 1968, *Perturbation Methods in Applied Mathematics*, Blaisdell, Waltham, 260 pp.
- Cunningham, P.M., R.T. Guza, and R.L. Lowe, 1979, Dynamic calibration of electromagnetic flow meters, *IEEE Oceans*, v 79, p 298-301.
- Davis, R.E. and L.A. Regier, 1977, Methods for estimating directional spectra from multi-element arrays, *J. Mar. Res.*, v 35, p 453-477.

- Feigenbaum, M.J., 1980, Universal behavior in nonlinear systems, Los Alamos Science, v 1, p 4-27.
- Flick, R.E., R.L. Lowe, M.H. Freilich, and J.C. Boylls, 1979, Coastal and laboratory wavestaff system, IEEE Oceans, v 79, p 623-625.
- Ford, J., 1974, The statistical mechanics of classical analytic dynamics, in *Fundamental Problems in Statistical Mechanics III*, Cohen, ed., Elsevier, p 215-256.
- Friedrichs, K.O., 1948, Water waves on a shallow sloping beach, *Comm. Pure and Appl. Math.*, v 1, p 109-134.
- Gable, C.G., 1979, Report on Data from the Nearshore Sediment Transport Study at Torrey Pines, Calif., Institute of Marine Resources ref. #79-8.
- Gragg, W.B., 1963, Repeated extrapolation to the limit in the numerical solution of ordinary differential equations, PhD. Thesis, UCLA, 103 pp.
- Grimshaw, R., 1970, The solitary wave in water of variable depth, *J. Fluid Mech.*, v 42, p 639-656.
- Guza, R.T. and E.B. Thornton, 1980, Local and shoaled comparisons of sea surface elevations, pressure, and velocities, *J. Geophys. Res.*, v 85, p 1524-1530.
- Hanson, E.T., 1926, The theory of ship waves, *Proc. Roy. Soc. London A*, v 111, p 491-529.
- Hasselmann, K., 1962, On the nonlinear energy transfer in a gravity wave spectrum, I, *J. Fluid Mech.*, v 12, p 481-500.
- Hasselmann, K., 1963, On the nonlinear energy transfer in a gravity wave spectrum, II, *J. Fluid Mech.*, v 15, p 273-281.
- Hasselmann, K., 1966, Feynman diagrams and interaction rules of wave-wave scattering processes, *Rev. Geophys. and Space Phys.*, v 4, p 1-32.
- Haubrich, R.A., 1965, Earth Noise, 5 to 500 millicycles per second, *J. Geophys. Res.*, v 70, p 1415.
- Herterich, K. and K. Hasselmann, 1980, A similarity relation for the nonlinear energy transfer in a finite-depth gravity-wave spectrum, *J. Fluid Mech.*, v 97, p 215-224.
- Inman, D.L., J.A. Zampol, T.E. White, D.M. Hanes, B.W. Waldorf, and K.A. Kastens, 1980, Field measurements of sand motion in the surf zone, *Proc. Conf. Coastal Eng. 17th, Amer. Soc. Civil Eng.*, v 2, p 1215-1234.

- Jenkins, G.M. and D.G. Watts, 1968, Spectral Analysis and its Applications, Holden-Day, San Francisco, 525 pp.
- Johnson, R.S., 1973, On the development of a solitary wave moving over an uneven bottom, Proc. Camb. Phil. Soc., v 73, p 183-203.
- Keller, J.B., 1948, The solitary wave and periodic waves in shallow water, Comm. Pure and Appl. Math., v 1, p 323-339.
- Korteweg, D.J. and G. DeVries, 1895, On the change in form of long waves advancing in a rectangular channel, and on a new type of long stationary waves, Phil. Mag., v 39, p 442.
- Lavelle, J.W., R.A. Yound, D.J. Swift, and T.L. Clarke, 1978, Near-bottom sediment concentration and fluid velocity measurements on the inner continental shelf, New York, J. Geophys. Res., v 83, p 6052-6062.
- LeMehaute, B. and L.M. Webb, 1964, Periodic gravity waves over a gentle slope at a third order approximation, Proc. Conf. Coastal Eng. 9th, Council on Wave Res., p 23-40.
- Longuet-Higgins, M.S., 1976, On the nonlinear transfer of energy in the peak of a gravity wave spectrum: a simplified model, Proc. Roy. Soc. London A, v 347, p 311-328.
- Lorenz, E.N., 1963, Deterministic nonperiodic flow, J. Atmos. Sci., v 20, p 130-141.
- Lowe, R.L., D.L. Inman, and B.M. Brush, 1972, Simultaneous data system for instrumenting the shelf, Proc. Conf. Coastal Eng. 13th, p 2.
- Mei C.C. and B. LeMehaute, 1966, Note on the equations of long waves over an uneven bottom, J. Geophys. Res., v 71, p 393.
- Mei, C.C. and U. Unluata, 1972, Harmonic generation in shallow water waves, in Waves on Beaches and Resulting Sediment Transport, Meyer, ed., Academic Press, New York, p 181-202.
- Miles, J.W., 1980, Solitary waves, Ann. Rev. Fluid Mech., v 12, p 22-43.
- Minorsky, N., 1974, Nonlinear Oscillations, Krieger, Huntington, 714 pp.
- Nayfeh, A.H., 1981, A comparison of perturbation methods for nonlinear Hyperbolic waves, in Singular Perturbations and Asymptotics, Meyer and Parter, eds., Academic Press, p 223-276.
- Newell, A.C., 1968, The closure problem in a system of random gravity waves, Rev. of Geophys., v 6, p 1-31.

- Pawka, S.S., D.L. Inman, R.L. Lowe, and L. Holmes, 1976, Wave Climate at Torrey Pines Beach, Ca., Tech. Paper 76-5, Coastal Eng. Res. Center, Fort Belvoir, 372 pp.
- Pawka, S.S., 1981, Wave directional characteristics on a partially sheltered coast, in preparation.
- Peregrine, D.H., 1967, Long waves on a beach, J. Fluid Mech., v 27, p 815-827.
- Peregrine, D.H., 1972, Equations for water waves and the approximations behind them, in Waves on Beaches and Resulting Sediment Transport, Meyer, ed., Academic Press, New York, p 95-122.
- Phillips, O.M., 1960, On the dynamics of unsteady gravity waves of finite amplitude, the elementary interactions, J. Fluid Mech., v 9, p 193-217.
- Phillips, O.M., 1977, The Dynamics of the Upper Ocean, Cambridge Univ. Press, London, 336 pp.
- Rayleigh, Lord, 1911, Hydrodynamical notes, Phil. Mag., v 21, p 177-195.
- Skjelbreia, L. and J. Hendrickson, 1960, Fifth order gravity wave theory, Proc. Conf. Coastal Eng. 7th, Council on Wave Res., p 184-196.
- Stoer, J., 1972, Extrapolation methods for the solution of initial value problems and their practical realization, in Lecture Notes in Mathematics, Dold and Ekman, eds., Springer-Verlag, v 362.
- Stoker, J.J., 1957, Water Waves, Interscience, New York, 567 pp.
- Stokes, G.G., 1847, On the theory of oscillatory waves, Trans. Cambridge Phil. Soc., v 8, p 441-455.
- Svendsen, Ib. A. and J.B. Hansen, 1978, On the deformation of periodic long waves over a gently sloping bottom, J. Fluid Mech., v 87, p 433-448.
- Whitham, G.B., 1974, Linear and Nonlinear Waves, John Wiley and Sons, New York, 636 pp.
- Whitham, G.B., 1979, Lectures on Wave Propagation, Tata Institute of Fundamental Research, Bombay, 148 pp.
- Willebrand, J., 1975, Energy transport in a nonlinear and inhomogeneous random gravity wave field, J. Fluid Mech., v 70, p 113-126.

